


RESEARCH ARTICLE

Open Access



# TRPA1 channels promote astrocytic $\text{Ca}^{2+}$ hyperactivity and synaptic dysfunction mediated by oligomeric forms of amyloid- $\beta$ peptide

Anthony Bosson<sup>1,2</sup>, Adrien Paumier<sup>1,2</sup>, Sylvie Boisseau<sup>1,2</sup>, Muriel Jacquier-Sarlin<sup>1,2</sup>, Alain Buisson<sup>1,2†</sup> and Mireille Albrieux<sup>1,2\*†</sup> 

## Abstract

**Background:** Excessive synaptic loss is thought to be one of the earliest events in Alzheimer's disease (AD). However, the key mechanisms that maintain plasticity of synapses during adulthood or initiate synapse dysfunction in AD remain unknown. Recent studies suggest that astrocytes contribute to functional changes observed during synaptic plasticity and play a major role in synaptic dysfunction but astrocytes behavior and involvement in early phases of AD remained largely undefined.

**Methods:** We measure astrocytic calcium activity in mouse CA1 hippocampus *stratum radiatum* in both the global astrocytic population and at a single cell level, focusing in the highly compartmentalized astrocytic arbor. Concurrently, we measure excitatory post-synaptic currents in nearby pyramidal neurons.

**Results:** We find that application of soluble A $\beta$  oligomers (A $\beta$ o) induced fast and widespread calcium hyperactivity in the astrocytic population and in the microdomains of the astrocyte arbor. We show that astrocyte hyperactivity is independent of neuronal activity and is repaired by transient receptor potential A1 (TRPA1) channels blockade. In return, this TRPA1 channels-dependent hyperactivity influences neighboring CA1 neurons triggering an increase in glutamatergic spontaneous activity. Interestingly, in an AD mouse model (APP/PS1–21 mouse), astrocyte calcium hyperactivity equally takes place at the beginning of A $\beta$  production, depends on TRPA1 channels and is linked to CA1 neurons hyperactivity.

**Conclusions:** Our experiments demonstrate that astrocytes contribute to early A $\beta$ o toxicity exhibiting a global and local  $\text{Ca}^{2+}$  hyperactivity that involves TRPA1 channels and is related to neuronal hyperactivity. Together, our data suggest that astrocyte is a frontline target of A $\beta$ o and highlight a novel mechanism for the understanding of early synaptic dysregulation induced by soluble A $\beta$ o species.

**Keywords:** Astrocyte, Calcium, Alzheimer, Synapse, TRPA1, APP/PS1

\* Correspondence: mireille.albrieux@univ-grenoble-alpes.fr

†Equal contributors

<sup>1</sup>University Grenoble Alpes, Grenoble Institut des Neurosciences, GIN, Chemin Fortuné Ferrini, BP170, F-38000 Grenoble, France

<sup>2</sup>Inserm, U1216, F-38000 Grenoble, France



## Background

Formation of toxic amyloid- $\beta$  (A $\beta$ ) species and their accumulation in plaques are key hallmarks in the pathogenesis of Alzheimer's disease (AD) but it has now been recognized that, far ahead of plaques formation, soluble A $\beta$  oligomers (A $\beta$ o) are the pathology-triggering species [1]. More specifically, A $\beta$ o manage a progressive loss of synaptic connectivity leading to neurodegeneration. Astrocytes are important safeguards of synaptic function and it becomes increasingly evident that these cells accomplish a more important role in brain function than previously thought. The loss of synapses may reflect functional downfall of astrocytes. These cells possess receptors and signaling machinery for all known neurotransmitters thus sensing neuronal activity [2]. They also actively secrete gliotransmitters such as ATP, glutamate, D-serine hence modulating activity of neuronal receptors [3, 4]. Consequently, through their involvement in the tripartite synapse, they both sense and modulate synaptic output [5].

Unlike neurons, astrocytes are electrically non-excitabile cells but they are equipped with numerous channels, receptors or exchangers triggering Ca<sup>2+</sup> signals. Thus, astrocytic excitability is based on highly spatiotemporally coordinated fluctuations of intracellular Ca<sup>2+</sup> concentration relying on plasmalemmal and intracellular channels [6]. Important progress has been made in studying astrocytes branches Ca<sup>2+</sup> signaling since they are the primary sites for interactions with neurons [7–9]. Direct monitoring of Ca<sup>2+</sup> dynamics in the processes of adult mouse hippocampal astrocytes has revealed intense local and compartmentalized activity that is dissociated from activity in the cell body [8]. However, until recently, it was difficult to specifically explore this astrocytic calcium activity since channels and receptors involved in astrocytic calcium signaling were commonly expressed in neurons. However, among the receptors involved in astrocytic calcium signaling, transient receptor potential A1 (TRPA1) channel seems to be specifically expressed in astrocytes and absent from neurons within hippocampus *stratum radiatum* [10, 11]. The discovery of TRPA1 channel as an important mediator of Ca<sup>2+</sup> entry restricted to astrocytes in the mouse hippocampus provided new opportunity to explore astrocyte signaling in relation to neuron-astrocyte interaction particularly in case of synaptic dysregulation.

In late transgenic AD mouse models, i.e. in phases associated with plaques formation, it has been shown that astrocytic calcium activity dramatically increases, becomes synchronous nearby A $\beta$  plaques and coordinates calcium signals at long distance [12]. Within somatosensory cortex, this astrocyte hyperactivity around plaques is mediated by purinergic signaling [13]. Surprisingly, astrocytes behavior and reactions in early

phases of AD remained largely undefined despite their probable involvement in the progressive loss of synaptic connectivity and in the complex and critical cellular phase of AD [14]. We thus chose to study the impact of soluble A $\beta$  oligomers on astrocytic function at the onset of early defensive cellular phase well before astrogliosis or inflammatory processes.

In this work, we monitored astrocytic calcium activity within the CA1 *stratum radiatum* region of the mouse hippocampus both at the astrocytic population level and at a single cell level, focusing in the astrocytic arbor. We characterized spontaneous Ca<sup>2+</sup> signaling properties at these two related levels and showed that A $\beta$ o exposition induced at once a global and a local Ca<sup>2+</sup> hyperactivity. We showed that this hyperactivity was independent of neuronal activity and was totally restored to physiological level by blocking TRPA1 channels. This TRPA1 channels-dependent influence of A $\beta$ o on astrocyte activity consequently impacted neighboring CA1 neurons, increasing glutamatergic spontaneous activity. In an AD mouse model, we showed that astrocyte hyperactivity was an early phenomenon setting up at the onset of A $\beta$  production, being also related to neuronal hyperactivity and preceding TRPA1 channel overexpression. Overall, our data provide a novel mechanism for the understanding of early toxicity of soluble A $\beta$ o species.

## Methods

### Slice preparation

Coronal hippocampal slices (ranging from 300 to 350  $\mu$ m thick) were prepared from Swiss mice (postnatal day 17–23; Janvier, Le Genest St Isle, France) or APP/PS1–21 transgenic mice [15] (postnatal day 19–28) together with control littermates. Mice were killed by decerebration and decapitated. The brain was rapidly removed and cut in ice-cold cutting ACSF containing (in mM): 2.5 KCl, 7 MgCl<sub>2</sub>, 0.5 CaCl<sub>2</sub>, 1.2 NaH<sub>2</sub>PO<sub>4</sub>, 25 NaHCO<sub>3</sub>, 11 D-glucose and 234 sucrose bubbled with 95% O<sub>2</sub> and 5% CO<sub>2</sub>, with a vibratome VT1200S (Leica, Wetzlar, Germany). Slices containing the hippocampus were placed in ACSF containing (in mM): 126 NaCl, 2.5 KCl, 1.2 MgCl<sub>2</sub>, 2.5 CaCl<sub>2</sub>, 1.2 NaH<sub>2</sub>PO<sub>4</sub> bubbled with 95% O<sub>2</sub> and 5% CO<sub>2</sub> and supplemented with 1 mM sodium pyruvate at room temperature for a recovery period.

### Slices bulk loading with Fluo-4 AM.

Briefly, 350  $\mu$ m coronal slices were loaded with the calcium indicator dye Fluo-4 by immersion for 45 min at 35 °C in a bath containing 5  $\mu$ M Fluo-4 AM (Life Technologies), 0.01% Pluronic acid F-127 (Molecular Probes), 0.005% Cremophor EL (Sigma-Aldrich) and 0.05% DMSO (dimethyl sulfoxide, Sigma-Aldrich) in

ACSF. The loading chamber was continuously oxygenated with 95% O<sub>2</sub> and 5% CO<sub>2</sub>. Slices were then transferred into dye-free ACSF for at least 45 min prior to experiments. Mainly live astrocyte took up the fluorescent dye with these conditions [16, 17].

#### Single-astrocyte dye loading with Fluo-4

Coronal 300 μm slices were transferred to a chamber allowing constant perfusion with ACSF at room temperature, bubbled with 95% O<sub>2</sub> and 5% CO<sub>2</sub> on the stage of an upright compound microscope (Eclipse E600 FN, Nikon, Paris, France) equipped with a water immersion 60× objective (NA 1.0) and an infrared-differential interference contrast optics with CCD camera (Optronix VX45, Kehl, Germany). Glass pipettes 8–11 MΩ (Harvard apparatus) were filled with intracellular solution containing (in mM): 105 K-gluconate, 30 KCl, 10 phosphocreatine, 10 HEPES, 4 ATP-Mg, 0.3 GTP-Tris, 0.2 Fluo-4 pentapotassium salt (Life Technologies), adjusted to pH 7.2 with KOH. Signals were amplified by Axopatch 200B, sampled by a Digidata 1440A interface and recorded with pClamp8 software (Molecular Devices, Foster City, USA). Astrocytes were identified based on morphological, localization in the *stratum radiatum* and negative resting potential (between -70 and -80 mV). Input resistance was calculated by measuring current in response to a 10 mV pulse with 80 ms duration, near the end of the voltage command. Only passive astrocytes showing linear *I/V* relationship and low input resistance (~ 50 MΩ) were kept for dye loading. After achieving whole-cell configuration, access resistance was constantly monitored, and astrocytes were excluded from this study when this parameter varied >20% throughout the experiment. To allow sufficient diffusion of the dye and avoid astrocyte dialysis, the time in whole-cell configuration was limited to less than 5 min. Then, the patch pipette was carefully withdrawn to allow the astrocyte to recover. In order to maximize the diffusion of the dye into the astrocytic processes, we waited at least 15 min before calcium imaging [8, 18].

#### Calcium imaging

Bulk or single-astrocyte loaded slices were placed in a constantly perfused chamber on the stage of an upright compound microscope (Eclipse E600 FN, Nikon, Paris, France) equipped with a water immersion 40× (NA 0.8) or 60× (NA 1.0) objective and a confocal head (confocal C1 head, Nikon, Paris, France). Excitation was achieved with light at 488 nm and emission was filtered with a 515 ± 15 nm filter. Images were acquired with EZ-C1 software (Nikon, Paris, France) at 1.2 s intervals in a single confocal plane over a period of 5 min.

#### Bulk loading calcium imaging data analysis

Prior to analysis, raw images were stabilized (when needed if slight *x-y* drift occurred during recordings, *z* drifts were excluded) using ImageJ plugin Template Matching. *CalSignal* software was used to measure intracellular Ca<sup>2+</sup> activity, analyzing the fluorescence signal *F* within each region of interest (ROI) corresponding to the cell body area of each astrocyte [19]. *F*<sub>0</sub> was calculated for each ROI on the recording period. Based on the Δ*F*/*F*<sub>0</sub> ratios, significant fluorescence variations were detected and a Ca<sup>2+</sup> event was defined as a significant and continuous signal increase larger than a fixed threshold followed by a significant and continuous signal decrease larger than the same threshold. Thus, cells were defined as active when fluorescence increased ≥2 standard deviations relative to baseline fluorescence. After peak detection, each Ca<sup>2+</sup> transients were visually checked by the operator. The theoretical Poisson distribution was calculated by the method of least squares approximating λ until it most closely fits the observed frequency distribution.

#### Single astrocyte loading data analysis

Ca<sup>2+</sup> transients were measured in two-dimensional images, in individual subregions matching the shape of the astrocyte structure. Manually selected ROIs (~1 μm<sup>2</sup>) were placed along astrocytic processes lying in the focal plane [8] and a ROI was also selected in the soma if accessible. Prior to analysis, raw images were stabilized (when needed if slight *x-y* drift occurred during recordings, *z* drifts were excluded) using ImageJ plugins Template Matching and filtered with 3D Hybrid Median Filter [7]. *CalSignal* software was used to measure intracellular Ca<sup>2+</sup> activity, analyzing the fluorescence signal *F* within each ROI. As described above, significant changes in fluorescence were detected on the basis of the calculated Δ*F*/*F*<sub>0</sub> ratios. Each Ca<sup>2+</sup> transients within ROI were visually checked by the operator and reported in a raster plot in order to discriminate focal activities from expanded ones (as described by [8]). At the end of each recording, *z*-stacks (0.5 μm steps) were performed to obtain tri-dimensional projections of astrocyte territories revealed by Fluo-4 loading. Images were then filtered with 3D Hybrid Median Filter plugin in ImageJ.

#### Electrophysiological recordings

Whole-cell recordings were made from the somata of visually identified CA1 pyramidal neurons. Patch pipettes (4–6 MΩ) were filled with an internal solution containing (in mM): 105 K-gluconate, 30 KCl, 10 phosphocreatine, 10 HEPES, 4 ATP-Mg, 0.3 GTP-Tris, 0.3 EGTA, adjusted to pH 7.2 with KOH. Spontaneous excitatory post-synaptic currents (sEPSCs) were collected at a membrane holding potential of -65 mV which is close to the reverse potential

of GABA. All recordings were done at room temperature (22–24 °C) and only a single neuron was studied per slice. sEPSCs and their kinetics were analyzed in 5-min epochs within the time frame of the recordings. Each epoch was compared to the initial 5-min recording and sEPSCs frequencies were normalized to this initial value. Access resistance was constantly monitored and recordings were excluded from this study when this parameter varied >20% throughout the experiment. Recordings were analyzed using the Clampfit module of the pClamp8 software (Molecular Devices, Foster City, USA) with a threshold at -20 pA to exclude miniature EPSCs.

#### **A $\beta$ oligomerization, monomer purification and drug application**

Recombinant A $\beta$ <sub>1–42</sub> peptide (Bachem) was resuspended in 1,1,1,3,3,3-hexafluoro-2-propanol (HFIP) to 1 mM until complete resuspension as described previously [20]. Following HFIP evaporation, A $\beta$  oligomers were prepared by diluting A $\beta$  to 1 mM in DMSO, then to 100  $\mu$ M in ice-cold ACSF with immediate vortexing and bath sonication, and then incubated at 4 °C for 24 h with mild agitation.

When appropriate, the A $\beta$  monomer is purified on a C18 column (SPE-Chromabond-HRX C18 ec, 200  $\mu$ l, 5 mg, Macherey-Nagel, France). The column was equilibrated with 0.1% trifluoroacetic acid (TFA) in water. Immediately after dilution in DMSO, the A $\beta$  sample was loaded and the column was washed three times with 0.1% TFA. Then, a gradient of acetonitrile from 30 to 60% was applied (Additional file 1). Fractions (0.1 ml) were collected. The elution profile was determined by measuring the absorbance at 275 nm. The peak fraction was collected and the concentration of peptide was determined by absorbance at 275 nm using  $\epsilon_{275 \text{ nm}} = 1400 \text{ M}^{-1} \text{ cm}^{-1}$ . The peptide is then stored at -80 °C.

A $\beta$ <sub>o</sub>, A $\beta$ <sub>m</sub>, tetrodotoxin (TTX; Latoxan, Valence, France), Ca<sup>2+</sup>-free solution (ACSF - 0 Ca<sup>2+</sup> - 1 mM EGTA) and HC 030031 (Sigma-Aldrich) were bath applied at the appropriate concentration during 5 min before and during calcium imaging or electrophysiological recordings. Minocycline hydrochloride (Sigma-Aldrich) was bath applied during 15 min before and during calcium imaging recording.

#### **Immunohistochemistry**

Mice were deeply anesthetized with 10% chloral hydrate and perfused intracardially with 10 ml 0.9% NaCl followed by 35 ml 4% paraformaldehyde in 0.1 M PBS, pH 7.3. Brains were rapidly removed, post-fixed overnight at 4 °C in 4% paraformaldehyde, immersed in 20% sucrose in 0.1 M PBS, pH 7.5 overnight, frozen in cooled (-35 °C) isopentane and stored at -30 °C. Serial frontal

sections (30  $\mu$ m thick) were cut with a cryostat microtome (HM 500 M, Microm, Francheville, France). Sections were blocked by incubation with 3% bovine serum albumin in TBS-Tween-Triton (TBSTT) (0.1 M Tris Base, 0.15 M NaCl, 0.1% Tween, 0.1% Triton X-100) for 30 min (dilution/blocking buffer). Tissue sections were then incubated overnight at 4 °C with either an anti-NeuN antibody (AbCys, France, mouse monoclonal; 1:500), anti-GFAP antibody (Molecular Probes, USA, mouse monoclonal; 1:1000), anti-TRPA1 antibody (Novus, USA, rabbit polyclonal; 1:100) or anti-Iba-1 antibody (Wako, USA, rabbit polyclonal; 1:500). Tissue sections were washed in TBSTT and incubated for 2 h at room temperature with Cyanin 3- (Jackson Immuno Research Laboratories, USA; 1:1000) or Alexa 488-conjugated secondary antibodies (Life Technology, USA; 1:1000). Sections were washed in TBSTT and mounted in Dako fluorescent mounting medium (Dako, USA).

When appropriate, amyloid- $\beta$  deposits were stained using Thioflavine S [21]. Sections were re-hydrated in TBS buffer (0.1 M Tris Base, 0.15 M NaCl), incubated in filtered 1% aqueous Thioflavine S (Sigma, France) for 8 min at room temperature, in the dark and washed several times in TBS buffer.

#### **Image acquisition**

Sections were examined with a Zeiss LSM 710 confocal laser scanning microscope with a Plan Apochromat 20 $\times$  objective (NA 0.8) or an oil immersion Plan Neofluor 40 $\times$  objective (NA 1.3) and translating platform with motorized crossed roller stages. When appropriate, mosaics were acquired for each channel separately with “Zen” software, in a 12-bit format, using the tile scan function. For TRPA1 and GFAP co-staining, sections were also acquired with a Zeiss Airyscan module with an oil immersion Plan Apochromat 63 $\times$  objective (NA 1.46) to improve lateral resolution (~140 nm) and signal-to-noise ratios. For illustration, images were merged with ImageJ software.

#### **Immunoblotting**

Dissected hippocampi from 1-month old APP/PS1-21 mice were homogenized in cold buffer containing 0.32 M sucrose and 10 mM HEPES, pH 7.4. Samples were maintained at 4 °C during all steps of the experiments. Homogenates were cleared at 1000  $\times$  g for 10 min to remove nuclei and large debris. Samples in loading buffer were boiled for 10 min and equal amounts of proteins (20  $\mu$ g, quantified by micro-BCA assay (Pierce) in duplicate extracts) were resolved on a 4–20% gradient Bis-Tris polyacrylamide precast stain free gels (Bio-Rad) in denaturing conditions. Proteins were transferred to a polyvinylidene difluoride membrane (Millipore) for 30 min at 4 °C. Membranes were

blocked with 3% dry milk in Tris-Buffered Saline (TBS: 10 mM Tris, 150 mM NaCl, pH 7.4) containing 0.1% Tween for 1 h at room temperature. Membranes were probed with anti-TRPA1 antibody (Novus, USA; 1:2000) and anti-GFAP antibody (Dako, USA, rabbit polyclonal; 1:100000) diluted in 3% dry milk in 0.1% Tween TBS overnight at 4 °C. Membranes were washed in 0.2% Tween TBS and probed with HRP-conjugated anti-rabbit IgG (Fab') (Interchim, France; 1:40,000) antibody for 45 min at room temperature. After washes, specific proteins were visualized with an enhanced chemiluminescence ECL Detection System (Bio-Rad) and the chemidoc system (Bio-Rad). Chemiluminescence signals were normalized to protein loading signals acquired using Stain-free pre-cast gels (Bio-Rad).

### Statistical analysis

Data were analyzed using R (the R Project for Statistical Computing) [22]. Comparisons between two groups were conducted with the two-tailed Mann-Whitney test. Kruskal-Wallis test followed by Pairwise comparison using Wilcoxon rank sum test was used when needed for multiple comparisons. Proportions of hyperactive/active astrocyte and focal/expanded activities were compared with  $\chi^2$ -test. Data were expressed as mean  $\pm$  SEM accompanied by distribution of experimental points. Graphic significance levels were \*,  $p < 0.05$ ; \*\*,  $p < 0.01$  and \*\*\*,  $p < 0.001$ .

## Results

### Ca<sup>2+</sup> activity in the astrocytic population and individual processes in mouse hippocampus

Ca<sup>2+</sup> signals encoding is known to be different in astrocytic cell body versus processes and involves different calcium sources such as internal stores release or external entry. Spatio-temporal Ca<sup>2+</sup> activity characteristics within astrocyte correlate to specific function associated with different territories. Astrocytes not only operate as individual cells but also take part in functional network through gap-junction coupling allowing remote communication in delimited functional brain area. We studied astrocytic Ca<sup>2+</sup> activity at once in the global astrocytic population and in single cell microdomains on mouse hippocampal slices (P17-P23) by using two complementary imaging techniques: i) Fluo-4 AM bulk loading to record calcium activity in the astrocytic population and ii) whole-cell patch-clamp technique to load individual astrocytes with Fluo-4 dye giving access to single cell processes territory (Additional file 2).

We analyzed signals by positioning regions of interest (ROIs) either in each cell body of Fluo-4 AM loaded astrocytes (20.0  $\pm$  1.3 ROIs by frame;  $n = 43$  slices from 14 animals in physiological condition; Fig. 1a, b) or by subdividing the entire patch-clamp loaded territory into subregions of similar area (1  $\mu\text{m}^2$ ; 111.7  $\pm$  7.3 ROIs by

astrocyte;  $n = 7$  astrocytes from 6 animals in physiological condition; Fig. 1e, f). These subregions corresponded to functional microdomains as previously defined by Di Castro et al. [8] since their size matched approximately the synaptic density in the neuropil region. We investigated some of the temporal properties of astrocytic Ca<sup>2+</sup> signals (such as the proportion of active cells, the proportion of active microdomains, the frequency of events) and some of the spatial properties of Ca<sup>2+</sup> signals within the astrocytic arbor (such as the events propagation).

In physiological condition, 49.1  $\pm$  2.2% of bulk loaded astrocytes were spontaneously active during a 5 min recording period ( $n = 43$  slices from 14 animals) with a mean frequency of 0.49  $\pm$  0.01 event/min ( $n = 817$  astrocytes; Fig. 1c). Frequency histograms revealed that the occurrence of Ca<sup>2+</sup> events in the astrocyte population was similar to a Poisson distribution with  $\lambda = 1.85$  suggesting that spontaneous Ca<sup>2+</sup> event within *stratum radiatum* was a stochastic phenomenon (Fig. 1d). Based on an in vivo study performed in mouse cortical astrocytes [13], we classified astrocytes as inactive (0 event/min), active (0.2–0.6 event/min) and hyperactive (> 0.6 event/min). We observed a minority of hyperactive astrocytes (11%) within mouse hippocampus *stratum radiatum* in physiological condition (Fig. 1d). This spontaneous activity is independent of neuronal activity since TTX (500 nM) had no effect on either the proportion of active astrocytes or the frequency of calcium activity or the proportion of active/hyperactive astrocyte (Fig. 2a–c). This therefore confirmed that the global activity of the astrocytic population is totally autonomous within the mouse hippocampus *stratum radiatum* [18]. In single patch-clamp loaded astrocyte, we had access to Ca<sup>2+</sup> activity in a two-dimensional acquisition plane representing on average 1945.3  $\pm$  140.1  $\mu\text{m}^2$  ( $n = 7$  astrocytes; Fig. 1e). We analyzed spatio-temporal encoding of Ca<sup>2+</sup> signals in 111.7  $\pm$  7.3 microdomains within the astrocytic arbor. In physiological condition, 57.9  $\pm$  4.8% of these microdomains were active (i.e. at least 1 Ca<sup>2+</sup> event; Fig. 1f, g) during a 5 min recording period with a mean activity frequency of 0.59  $\pm$  0.01 event/min ( $n = 782$  ROIs). As previously described in mouse dentate gyrus astrocytes [8], we identified two types of Ca<sup>2+</sup> events: “focal events” that are confined to 1 to 4 microdomains and “expanded events” appearing in more than 4 contiguous subregions (Fig. 1h). An additional movie file shows these two types of events in more details (Additional file 3). Focal events were the large majority (67%) occurring randomly in all subregions. Expanded events arose less often (33%) and spread over 7.1  $\pm$  0.4  $\mu\text{m}^2$ . Within *stratum radiatum*, these two types of Ca<sup>2+</sup> event were independent of neuronal activity since

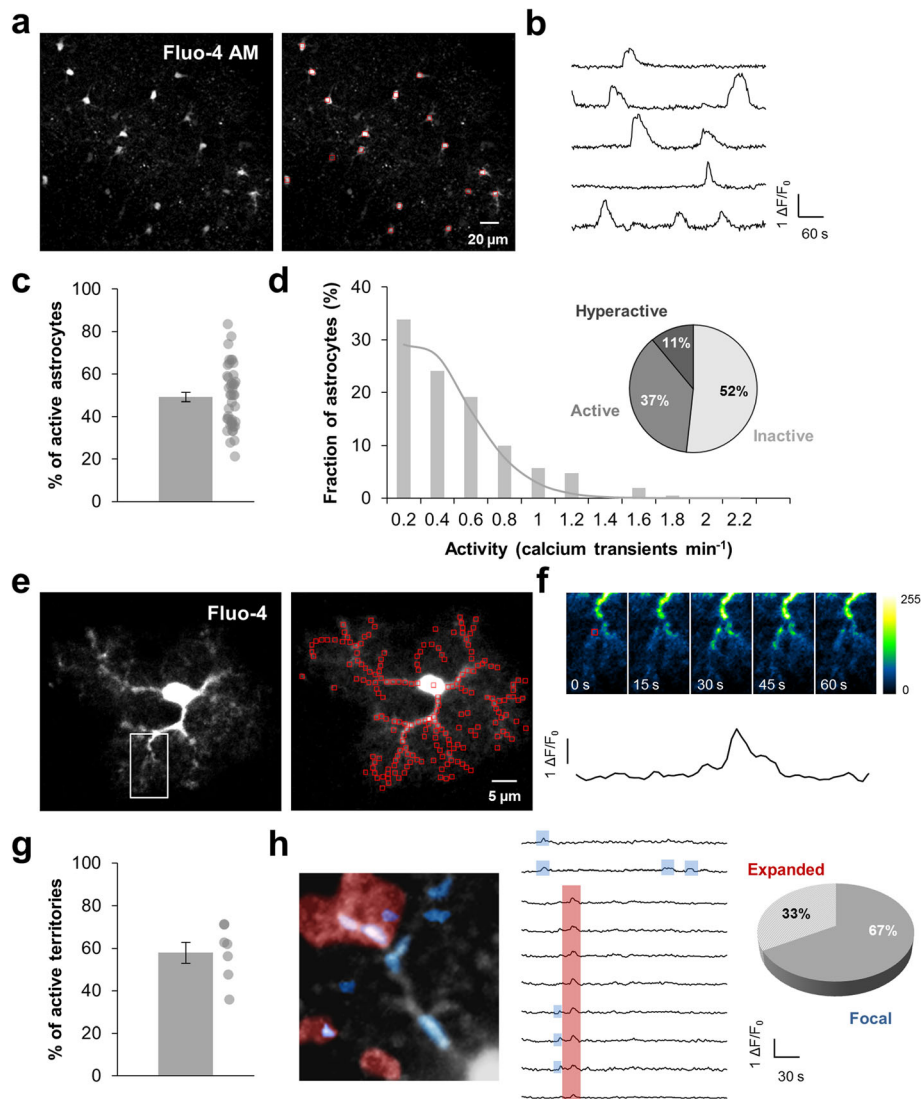
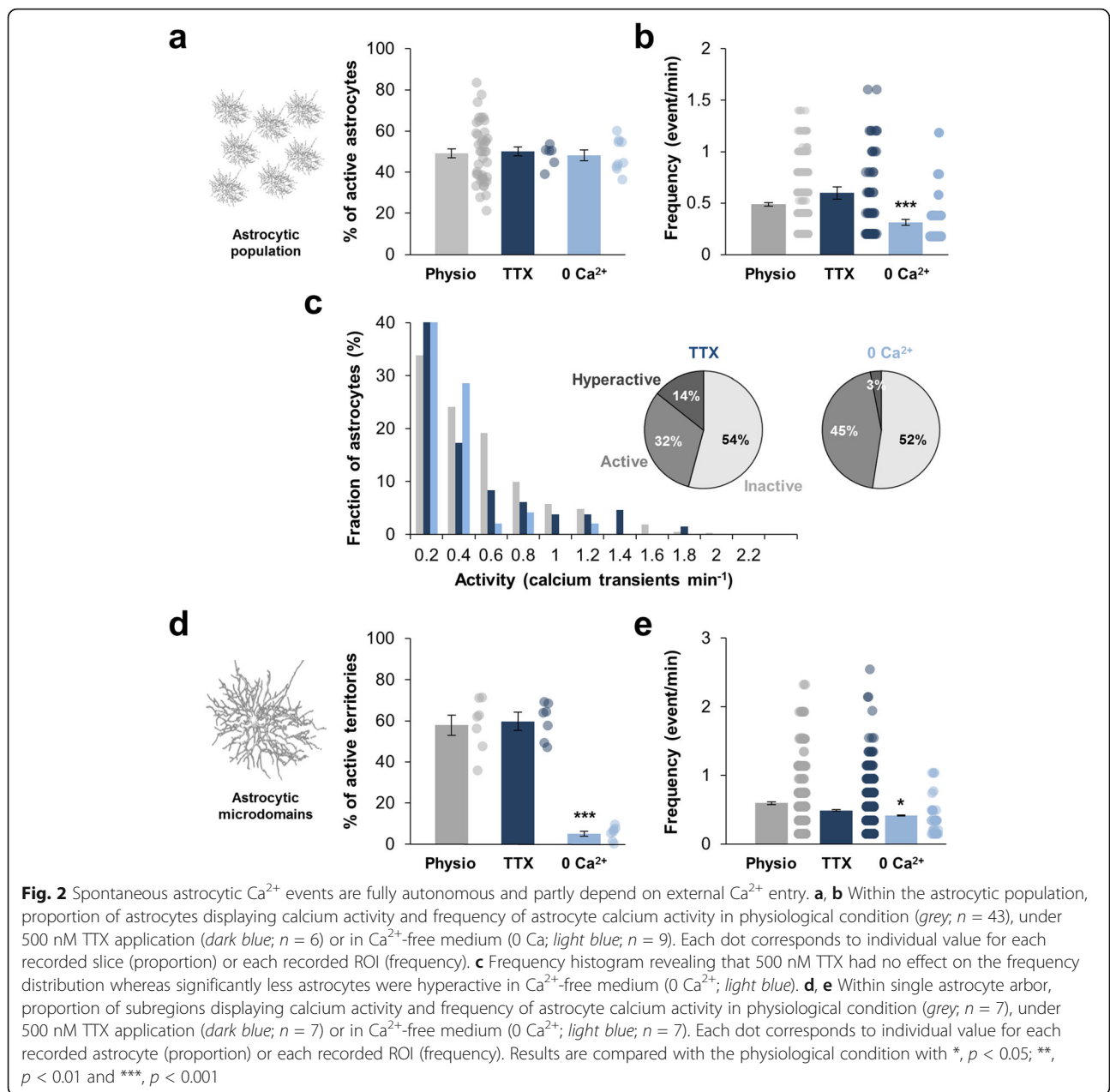


**Fig. 1** Detection of global and compartmentalized  $\text{Ca}^{2+}$  events in astrocytes. **a** Fluo-4-loaded astrocytes in the *stratum radiatum* of a mouse coronal slice. Fluorescence variations were analyzed in astrocyte cell bodies (red square). **b** Example of typical fluorescence variations recorded in physiological condition. **c** Proportion of astrocytes displaying calcium activity during a 5-min recording. Each dot corresponds to individual value for each recorded slice ( $n = 43$ ). **d** Frequency histogram showing the occurrence of  $\text{Ca}^{2+}$  events in the astrocyte population and the related theoretical Poisson distribution (grey curve). Pie chart representing inactive (0 event per min), active (0.2–0.6 event per min) and hyperactive ( $> 0.6$  event per min) astrocytes in physiological condition. **e** Single patch-clamp Fluo-4-loaded astrocyte in the *stratum radiatum* of a mouse coronal slice. Fluorescence variations within processes were analyzed in subregions of  $\sim 1 \mu\text{m}^2$  (red square) in a single z-plane. **f** Time-lapse  $\text{Ca}^{2+}$  imaging in an astrocyte process showing an example of  $\text{Ca}^{2+}$  event. Time between frames, 15 s. The black curve corresponded to the fluorescence signal recorded in a selected ROI (red square, first image). **g** Proportion of subregions displaying a calcium activity during a 5-min recording. Each dot corresponds to individual value for each recorded astrocyte ( $n = 7$ ). **h** Artificial color superposition of focal  $\text{Ca}^{2+}$  events (1–4 contiguous subregions, blue) and expanded  $\text{Ca}^{2+}$  events ( $> 4$  contiguous subregions, red) occurring during a 5-min recording in an astrocyte process, as defined by [8]. Traces showing occurrence of  $\text{Ca}^{2+}$  peaks in contiguous subregions with blue and red highlights identifying focal (blue) and expanded (red)  $\text{Ca}^{2+}$  events respectively. In physiological condition, focal events represent the major part of  $\text{Ca}^{2+}$  events within the astrocytic processes

TTX application didn't affect either the proportion or the frequency of focal and expanded events (Fig. 2d, e).

Astrocytic  $\text{Ca}^{2+}$  signaling involves both internal  $\text{Ca}^{2+}$  stores and external  $\text{Ca}^{2+}$  entry. Within the *stratum radiatum* astrocyte population, removal of external  $\text{Ca}^{2+}$

from the bath (ACSF - 0  $\text{Ca}^{2+}$  - EGTA 1 mM) had no effect on the proportion of spontaneously active astrocytes ( $48.2 \pm 2.7\%$  in  $\text{Ca}^{2+}$ -free medium vs  $49.1 \pm 2.2\%$  in ACSF;  $n = 9$  slices from 5 animals;  $p = 0.97$ ) but aborted approximately 35% of events within active cells



( $0.31 \pm 0.02$  event/min in Ca<sup>2+</sup>-free medium vs  $0.48 \pm 0.01$  in physiological condition; *n* = 103 astrocytes; *p* < 0.0001) meaning that one third of somatic Ca<sup>2+</sup> events depended on a Ca<sup>2+</sup> entry (Fig. 2a–c). Particularly, the proportion of hyperactive/active astrocytes was strongly affected (3% of hyperactive astrocytes versus 11% in physiological condition; *p* < 0.001). Yet, location of internal stores is not uniformly distributed in the astrocytic territory since they are concentrated in cell body and thick processes, thin astrocytic processes being practically devoid of Ca<sup>2+</sup> stores [23]. Consistently, we observed that removing external Ca<sup>2+</sup> suppressed nearly all the compartmentalized Ca<sup>2+</sup> transients in the astrocytic arbor

( $5.1 \pm 1.3\%$  active territories vs  $57.8 \pm 4.8\%$  in physiological condition; *n* = 7 astrocytes from 6 animals; *p* = 0.0006) and reduced the frequency of the residual signals ( $0.41 \pm 0.01$  event/min vs  $0.59 \pm 0.01$  in physiological condition; *n* = 687 ROIs; *p* = 0.04) (Fig. 2d, e).

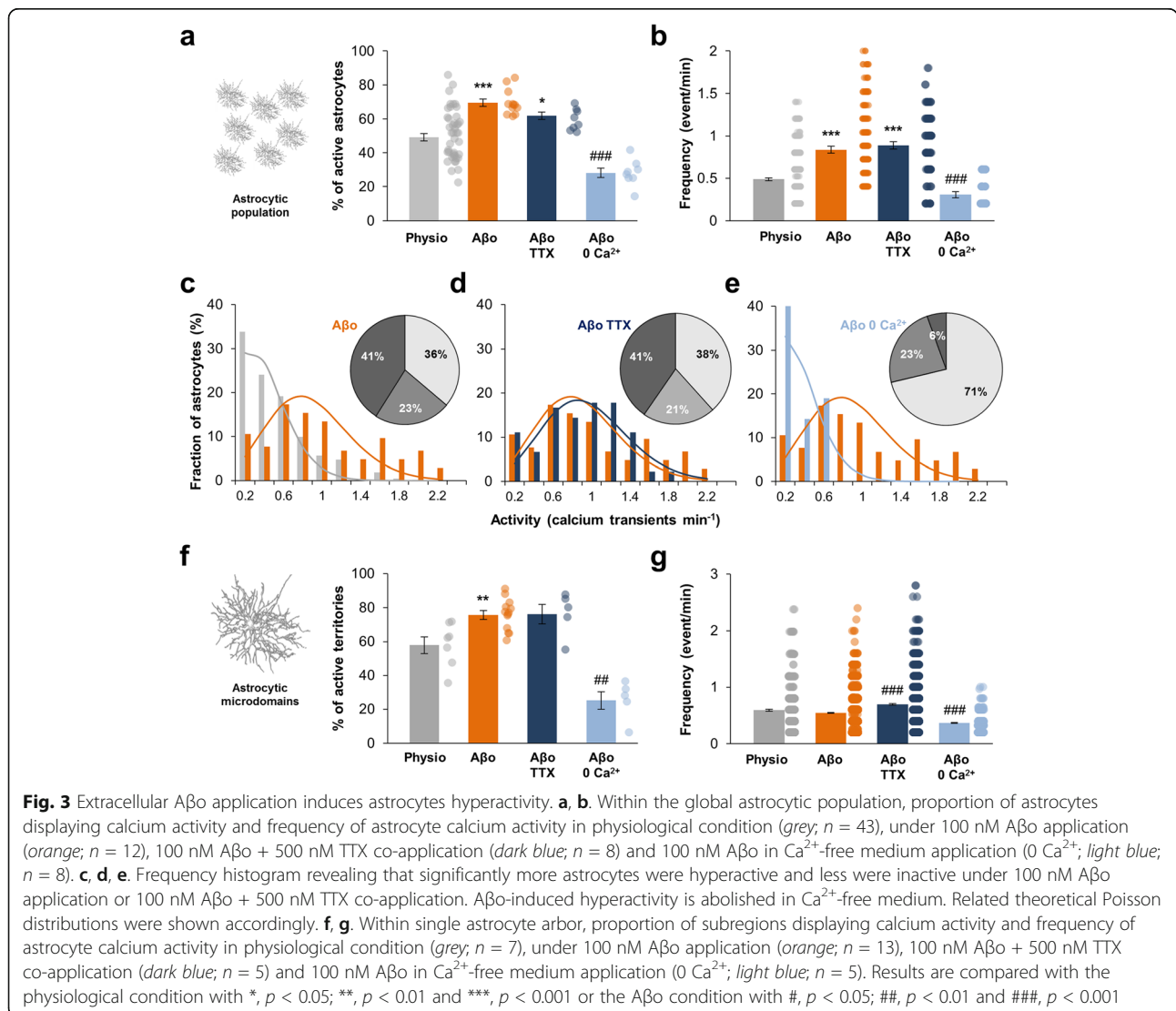
#### Astrocytes become hyperactive in presence of amyloid-β oligomers

To investigate the effect of soluble Aβ<sub>1–42</sub> oligomers (Aβ<sub>o</sub>) on astrocytic calcium signaling, we perfused hippocampal slices with 100 nM of oligomeric forms of the peptide during 5 min before recording. In the global astrocytic population, application of Aβ<sub>o</sub> resulted in a

significant increase in the proportion of active astrocytes ( $69.7 \pm 2.1\%$  vs  $49.1 \pm 2.2\%$  in physiological condition;  $n = 12$  slices;  $p < 0.0001$ ; Fig. 3a). Within active cells, the frequency of  $Ca^{2+}$  events also significantly rose ( $0.83 \pm 0.04$  event/min vs  $0.48 \pm 0.01$  event/min in physiological condition;  $n = 237$  astrocytes;  $p < 0.0001$ ; Fig. 3b). Frequency histogram was switched to high frequency and developed differently from the basal Poisson distribution ( $\lambda = 4.39$ ; Fig. 3c). This suggested that  $Ca^{2+}$  event was not anymore a stochastic phenomenon but was managed by  $A\beta$ . The fraction of hyperactive astrocyte (i.e.  $> 0.6$  event/min) was significantly larger (41% in  $A\beta$  condition vs 11% in physiological condition;  $p = 0.012$ ; Fig. 3c). Thus, under application of 100 nM  $A\beta$ , there is an increase in the population of hyperactive astrocytes at the expense of basal-active and -inactive astrocytes.

In individual patch-clamped astrocyte, application of  $A\beta$  induced a significant increase of the fraction of active territories ( $75.8 \pm 2.5\%$  vs  $57.9 \pm 4.8\%$  in physiological condition;  $n = 13$  astrocytes;  $p = 0.0055$ ; Fig. 3f) with no effect on the frequency of  $Ca^{2+}$  events within these microdomains ( $0.54 \pm 0.01$  vs  $0.59 \pm 0.02$  event/min;  $n = 1806$  ROIs;  $p = 0.178$ ; Fig. 3g). Both focal and expanded event numbers were increased and the ratio of expanded/focal  $Ca^{2+}$  events was not significantly affected by  $A\beta$  (41% of expanded events in  $A\beta$  condition vs 33% in physiological condition;  $p = 0.27$ ; Additional file 4a). However, expanded events size significantly increased compared to physiological condition ( $9.2 \pm 0.5 \mu m^2$  vs  $7.1 \pm 0.4 \mu m^2$ ;  $p = 0.045$ ; Additional file 4c).

Application of monomeric forms of  $A\beta_{1-42}$  ( $A\beta m$ ) had no effect on either the proportion of active cells or the  $Ca^{2+}$  signal properties within cells confirming that only





oligomeric forms of A $\beta$  were responsible for this Ca<sup>2+</sup> hyperactivity ( $n = 14$  slices from 4 animals; Additional file 1c). Major oligomers present in our samples were low-molecular weight oligomers (2- to 4- mers; Additional file 1a).

Thus, 100 nM A $\beta$  triggered astrocytic calcium hyperactivity within the *stratum radiatum* as soon as 5 min in the global astrocytic population, manifested as an increase of the proportion of active cells along with an increase of the frequency of individual Ca<sup>2+</sup> events. Interestingly, this global hyperactivity went along with a sustained increase of Ca<sup>2+</sup> activity within astrocytic processes including an increase of the proportion of active microdomains together with an increase of the expanded events size in the astrocytic processes.

**A $\beta$ -induced astrocytic Ca<sup>2+</sup> hyperactivity is independent of neuronal activity or microglia activation and involves external Ca<sup>2+</sup> entry**

A $\beta$  could potentially affect directly and/or indirectly Ca<sup>2+</sup> signaling within astrocytes. In order to ascertain the neuronal part in the astrocyte hyperactivity, we co-applied 500 nM TTX with 100 nM A $\beta$ . In bulk loading condition, TTX had no effect on the A $\beta$ -induced astrocytic Ca<sup>2+</sup> hyperactivity either in the proportion of active astrocytes ( $61.9 \pm 2.2\%$ ;  $n = 8$  slices from 6 animals; Fig. 3a) or in the frequency of Ca<sup>2+</sup> events ( $0.89 \pm 0.04$  event/min;  $n = 145$  astrocytes; Fig. 3b). The proportion of hyperactive astrocytes was similar ( $p = 0.16$ ) and the frequency distribution was not impacted by TTX application (Fig. 3d). In the same way, in individual patch-clamped astrocyte, the blockade of action potentials with TTX did not affect the A $\beta$  effect on the proportion of active territories ( $n = 5$  astrocytes from 4 animals;  $p = 1.0$ ; Fig. 3f) and on the frequency of Ca<sup>2+</sup> events ( $n = 870$  ROIs;  $p = 0.9$ ; Fig. 3g). The enlarged size of expanded events was not reduced with TTX ( $9.0 \pm 0.5 \mu\text{m}^2$ ;  $p = 0.68$ ; Additional file 4c). These data suggested that, within 5 min, A $\beta$  acts directly on astrocyte signaling independently of any neuronal activity.

Activation of microglia can be a relatively early event in the A $\beta$  mediated pathological process and can in turn activate astroglia cells [24, 25]. In order to assess the role of microglia in the A $\beta$ -induced astrocytic Ca<sup>2+</sup> hyperactivity, we pretreated slices with minocycline, an inhibitor of microglia activation [24–26]. Minocycline 50 nM pre-incubated during 15 min did not prevent the ability of A $\beta$  to trigger astrocytic Ca<sup>2+</sup> hyperactivity increasing to the same extent the proportion of active astrocytes ( $61.0 \pm 3.3\%$ ;  $n = 6$  slices from 4 animals;  $p = 0.0043$ ) and the frequency of Ca<sup>2+</sup> events ( $0.79 \pm 0.08$  event/min;  $n = 69$  astrocytes;  $p = 0.02$ ; Additional file 5a). Thus,

within 5 min, A $\beta$  acts directly on astrocyte signaling independently of any microglia activation.

To investigate the external and/or internal origin of Ca<sup>2+</sup> implicated in the A $\beta$ -induced Ca<sup>2+</sup> hyperactivity, we applied 100 nM A $\beta$  in Ca<sup>2+</sup>-free ACSF. Within the astrocytic population, we observed a 60% decrease of the proportion of active astrocytes ( $28.1 \pm 2.7\%$  active astrocytes in Ca<sup>2+</sup>-free medium versus  $69.7 \pm 2.1\%$  in ACSF;  $n = 8$  slices from 6 animals;  $p = 0.0002$ ; Fig. 3a). The A $\beta$ -induced frequency increase of Ca<sup>2+</sup> events was also strongly reduced in Ca<sup>2+</sup>-free medium ( $0.30 \pm 0.03$  event/min;  $n = 73$  astrocytes;  $p < 0.0001$ ; Fig. 3b) and the proportion of hyperactive cells strongly declined (6% vs 41%;  $p < 0.0001$ ; Fig. 3e). Within astrocytic processes, removing external Ca<sup>2+</sup> avoided 1/3 of compartmentalized A $\beta$ -induced Ca<sup>2+</sup> hyperactivity ( $25.2 \pm 5.2\%$  of active territories;  $n = 5$  astrocytes from 4 animals;  $p = 0.0016$ ; Fig. 3f) and strongly reduced the frequency of the remaining signals ( $0.37 \pm 0.01$  event/min;  $n = 870$  ROIs;  $p < 0.0001$ ; Fig. 3g). The enlarged size of expanded events was however not significantly reduced in Ca<sup>2+</sup>-free medium ( $7.7 \pm 0.7 \mu\text{m}^2$ ;  $p = 0.7$ ; Additional file 4c). Overall, these data suggested that external Ca<sup>2+</sup> entry is the main source of A $\beta$ -induced Ca<sup>2+</sup> hyperactivity in the astrocytic population and in the astrocytic processes, superimposing a new signal encoding.

**TRPA1 channels underlie Ca<sup>2+</sup> hyperactivity induced by A $\beta$**

Within astrocyte, Ca<sup>2+</sup> entry can occur through astrocytic ligand-gated Ca<sup>2+</sup> channels (ionotropic receptors), transient receptor potential (TRP) receptors and reverse operation of Na<sup>+</sup>/Ca<sup>2+</sup> exchanger (NCX). Astrocytic cationic ionotropic receptors (such as AMPA, NMDA or P2X receptors) have relatively low single channel conductance (~1 to 3 pS) and accounted for ~4% of fractional Ca<sup>2+</sup> current [6]. Among TRP receptors, TRPA1 channels have been recently involved in regulating astrocyte basal Ca<sup>2+</sup> levels in the hippocampus *stratum radiatum* [10, 11]. Interestingly, TRPA1 channels have a relatively high single channel conductance (~110 pS) accounting for ~17% of fractional Ca<sup>2+</sup> current for the constitutively open channel [27] referring them as important actors involved in astrocytic Ca<sup>2+</sup> entry. Within the CA1 region of mouse hippocampus, functional TRPA1 were only detected in astrocytes [10]. Based on immunohistochemistry of fixed brain sections, we found that TRPA1 channels staining appeared as discrete punctates predominantly co-localized with astrocytes (GFAP-positive cells; Additional file 6). Higher-resolution images showed that TRPA1 channels were expressed in both cell body and thick processes of *stratum radiatum* astrocytes objectivized by the GFAP co-staining. Some staining also appeared in adjacent

territories (Fig. 4a) continuous with GFAP-positive stem processes. An additional 3D-reconstruct movie file shows this in more details (Additional file 7) and suggested that TRPA1 channels were expressed in astrocyte thin processes. These observations agreed with immunogold electron microscopy studies performed in rat trigeminal caudal nucleus showing that TRPA1 channels are localized in astrocyte peripheral processes [28].

In physiological condition, incubation of slices with the selective TRPA1 blocker, HC 030031 (40  $\mu$ M) [29], during 5 min had no effect on the proportion of

spontaneous active astrocytes within the global astrocytic population ( $56.5 \pm 3.5\%$  active astrocytes;  $n = 7$  slices from 3 animals;  $p = 0.17$ ; Fig. 4b) but increased the frequency of  $Ca^{2+}$  events ( $0.56 \pm 0.03$  event/min;  $n = 167$  astrocytes;  $p = 0.043$ ; Fig. 4c). In patch-clamped cells, incubating 5 min slices with 40  $\mu$ M HC 030031 had no impact on the proportion of active microdomains ( $62.8 \pm 5.7\%$ ;  $n = 7$  astrocytes from 4 animals;  $p = 0.71$ ; Fig. 4e) or on  $Ca^{2+}$  signal frequency ( $0.50 \pm 0.01$  event/min;  $n = 919$  ROIs;  $p = 0.19$ ; Fig. 4f). Together, these data confirmed that TRPA1 does not massively

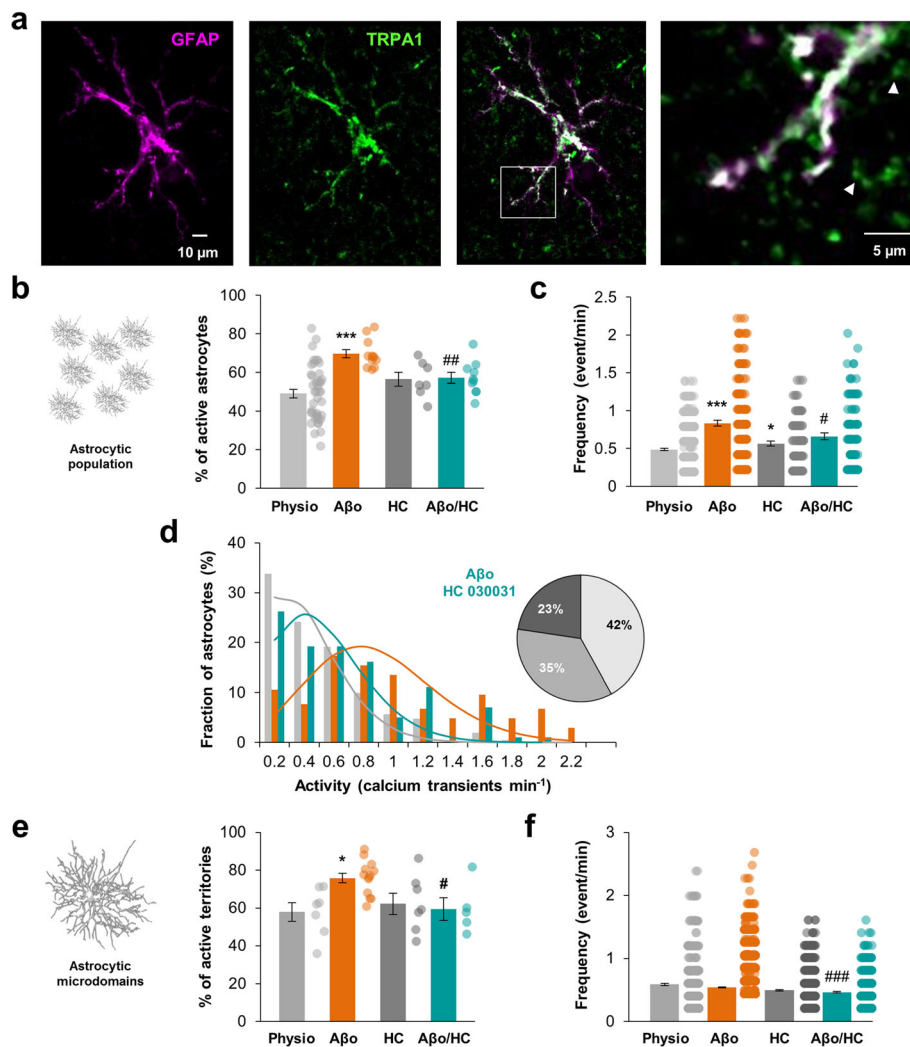


**Fig. 4** TRPA1 channels mediate astrocytic hyperactivity. **a** Immunohistochemistry of mouse *stratum radiatum* astrocytes showing that TRPA1 channels expression (green) was located in GFAP-positive processes (magenta) but also went over in distal processes excluding GFAP staining (e.g. white arrowheads). **b, c.** Within the astrocytic population, proportion of astrocytes displaying calcium activity and frequency of astrocyte calcium activity in physiological condition (light grey;  $n = 43$ ), under 100 nM A $\beta$  application (orange;  $n = 12$ ), 40  $\mu$ M HC 030031 application (dark grey;  $n = 7$ ) and 100 nM A $\beta$  + 40  $\mu$ M HC 030031 co-application (cyan;  $n = 10$ ). **d** Frequency histogram revealing that A $\beta$ -induced hyperactivity is reduced when HC 030031 is co-applied (cyan). Related theoretical Poisson distributions were shown accordingly. **e, f.** Within single astrocyte arbor, proportion of subregions displaying calcium activity and frequency of astrocyte calcium activity in physiological condition (light grey;  $n = 7$ ), under 100 nM A $\beta$  application (orange;  $n = 13$ ), 40  $\mu$ M HC 030031 application (dark grey;  $n = 7$ ) and 100 nM A $\beta$  + 40  $\mu$ M HC 030031 co-application (cyan;  $n = 5$ ). Results are compared with the physiological condition with \*,  $p < 0.05$ ; \*\*,  $p < 0.01$  and \*\*\*,  $p < 0.001$  or the A $\beta$  condition with #,  $p < 0.05$ ; ##,  $p < 0.01$  and ###,  $p < 0.001$

contribute to spontaneous  $\text{Ca}^{2+}$  signaling in the astrocytic arbor territory of *stratum radiatum* astrocytes [11, 30].

Interestingly, when  $\text{A}\beta$  was applied in presence of HC 030031 (40  $\mu\text{M}$ ), the astrocytic  $\text{Ca}^{2+}$  hyperactivity was totally abolished and restored to basal levels either in the global astrocytic population or in the processes territory. In bulk loading condition, the proportion of active astrocytes decreased ( $57.1 \pm 2.8\%$  in  $\text{A}\beta$  + HC 030031 vs  $69.7 \pm 2.1\%$  in  $\text{A}\beta$  condition;  $n = 10$  slices from 3 animals;  $p = 0.0021$ ; Fig. 4b) and was reversed to physiological condition level ( $49.1 \pm 2.2\%$ ;  $p = 0.08$ ). Frequency also decreased when HC 030031 was co-applied with  $\text{A}\beta$  ( $0.67 \pm 0.04$  event/min vs  $0.83 \pm 0.04$  event/min in  $\text{A}\beta$  condition;  $n = 181$  astrocytes;  $p = 0.013$ ; Fig. 4c) but remained higher than in physiological condition ( $0.49 \pm 0.01$  event/min;  $p = 0.0002$ ). Frequency distribution tended toward physiological distribution and the proportion of hyperactive astrocytes was reduced (23% in  $\text{A}\beta$  + HC 030031 vs 41% in  $\text{A}\beta$  condition;  $p = 0.023$ ; Fig. 4d). Within individual cells, the proportion of active microdomains declined ( $59.4 \pm 6.0\%$  of active microdomains in  $\text{A}\beta$  + HC 030031 vs  $75.8 \pm 2.5\%$  in  $\text{A}\beta$  condition;  $n = 5$  astrocytes from 4 animals;  $p = 0.03$ ) close to physiological value ( $57.9 \pm 4.8\%$ ;  $p = 0.87$ ; Fig. 4e) together with the events frequency ( $0.47 \pm 0.09$  event/min in  $\text{A}\beta$  + HC 030031 vs  $0.54 \pm 0.07$  event/min in  $\text{A}\beta$  condition;  $n = 760$  ROIs;  $p < 0.0001$ ; Fig. 4f). The ratio of expanded/focal event decreased (30% of expanded event in  $\text{A}\beta$  + HC 030031 vs 41% in  $\text{A}\beta$  condition;  $p = 0.039$ ; Additional file 4a) reaching physiological value (33%;  $p = 0.45$ ). Expanded surface extension also shrank ( $7.2 \pm 0.5 \mu\text{m}^2$  vs  $9.2 \pm 0.5 \mu\text{m}^2$ ;  $p = 0.017$ ; Additional file 4c) close to physiological size ( $7.1 \pm 0.4 \mu\text{m}^2$ ).

Thus, while having a negligible impact on physiological spontaneous  $\text{Ca}^{2+}$  activity, blocking TRPA1 channels cancelled astrocyte  $\text{Ca}^{2+}$  hyperactivity induced by  $\text{A}\beta$  leading most of the spatiotemporal  $\text{Ca}^{2+}$  signal properties back to physiological state in either the astrocytic arbor microdomains or the global astrocytic population.

#### APP/PS1-21 mice display early astrocytic hyperactivity that involves TRPA1 channels

APP/PS1-21 mice co-express the human KM/67/671NL mutation in the amyloid precursor protein (APP<sup>swe</sup>) and the human L166P-mutated presenilin 1 (PS1) under the control of Thy1 promotor. These transgenic mice display high transgene expression with  $\text{A}\beta_{1-42}$  levels being significant at 1 month and plaques appearing at 6 weeks of age in the neocortex and at 4–5 months in the CA1 hippocampus [15]. As external application of  $\text{A}\beta$  induced an immediate astrocytic hyperactivity in hippocampal healthy brain slices, we wonder about the

effect of  $\text{A}\beta$  in APP/PS1-21 mice at the beginning of its secretion within the brain. Thy1 is known to be expressed from ~P14 in mouse CA1 hippocampus [31] thus  $\text{A}\beta_{1-42}$  might be produced from this stage. However, while being present at this early stage [15],  $\text{A}\beta$  were not yet aggregated in plaques in APP/PS1-21 mice at 1-month-old (Fig. 5a) while  $\text{A}\beta$  plaques were present in the hippocampus at 6-month-old as testified with Thioflavin S labeling [21]. Likewise, astroglial marker such as GFAP showed a similar profile in WT versus APP/PS1-21 mice at 1-month-old confirming the lack of reactive astrogliosis in these early stages (Fig. 5b, d). Thus, studying astrocyte activity at these early stages allowed us to measure the impact of not aggregated  $\text{A}\beta$  on healthy astrocytes in an AD transgenic mice model.

We first investigated the expression of TRPA1 channels in the hippocampus of young APP/PS1-21 mice and their littermates (WT). We found that the protein level of TRPA1 channels was similar in P19 mice ( $n = 6$  hippocampus from 3 animals for each;  $p = 0.9$ ; Fig. 5c) and twice higher in P30 APP/PS1-21 than WT mice ( $n = 8$  hippocampus from 4 animals for each;  $p = 0.02$ ; Fig. 5c) suggesting an early upregulation of this channel from the onset of  $\text{A}\beta$  secretion. At the same time, GFAP protein level was stable (Fig. 5d) testifying the lack of astrogliosis in these early AD stages.

We then recorded astrocytic  $\text{Ca}^{2+}$  signals in young APP/PS1-21 mice (from P19 to P28) and compared to their littermates (WT). In bulk loaded slices, the proportion of active astrocytes within *stratum radiatum* was similar in both condition ( $45.4 \pm 4.1\%$  in APP/PS1-21 vs  $47.1 \pm 4.9\%$  in WT;  $n = 8$  slices from 5 animals in each condition;  $p = 0.8$ ; Fig. 6a). However, the frequency of  $\text{Ca}^{2+}$  events was significantly higher in APP/PS1-21 cells ( $0.65 \pm 0.07$  event/min in APP/PS1-21 vs  $0.33 \pm 0.03$  event/min in WT;  $n = 103$  and  $105$  astrocytes respectively;  $p = 0.0013$ ; Fig. 6a) and the frequency distribution was switched to higher frequency in APP/PS1-21 compared to WT mice ( $\lambda = 2.1$  vs  $1.21$  in WT; Fig. 6b) leading to an increase of the fraction of hyperactive cells (21% vs 6% in WT;  $p = 0.0009$ ; Fig. 6b).

In this AD mouse model, no signs of neuroinflammation were apparent in 1-month-old mice and microgliosis has been described to be concomitant with plaques appearance [15]. Indeed, at these early stages, microglia phenotype was not different in APP/PS1-21 mice from WT littermate (Iba-1 immunostaining; Additional file 5b). However, to confirm that microglia was not involved in these early astrocytic events, we pretreated slices with minocycline in order to inhibit potential microglia activation [24–26]. Minocycline 50 nM, pre-incubated during 15 min, had no effect on either the proportion of active cells or the frequency of astrocytic  $\text{Ca}^{2+}$  events within

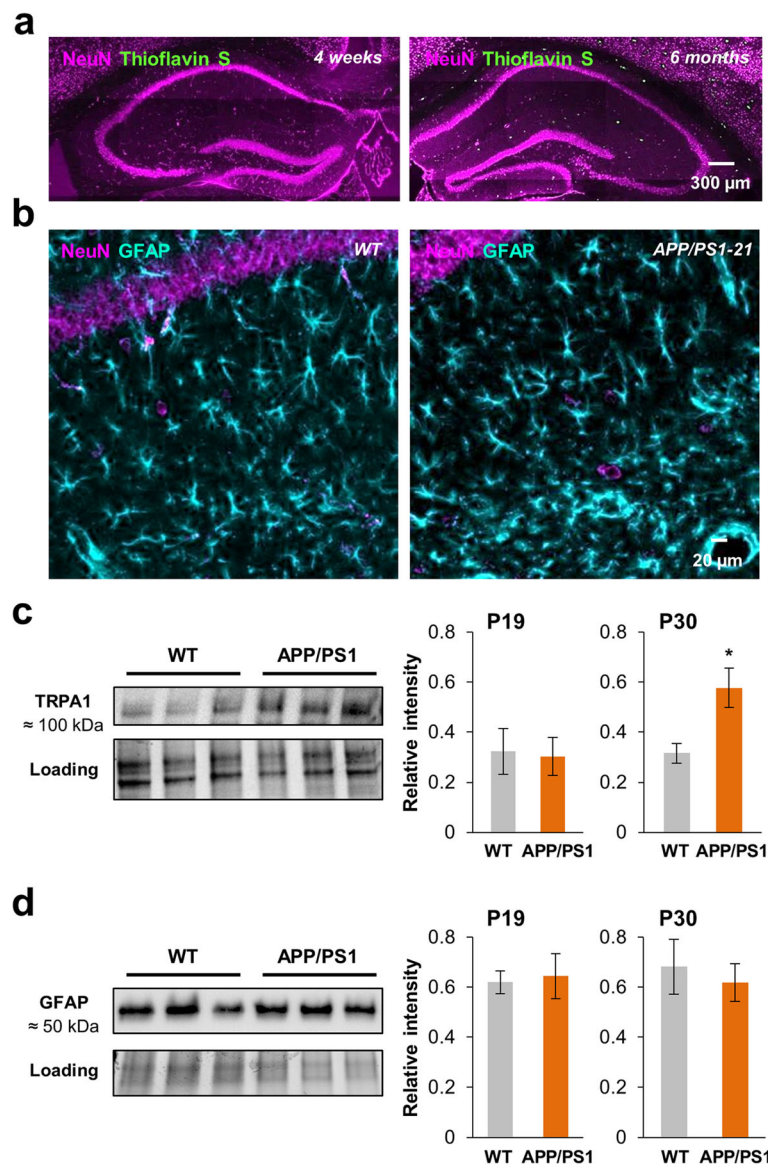
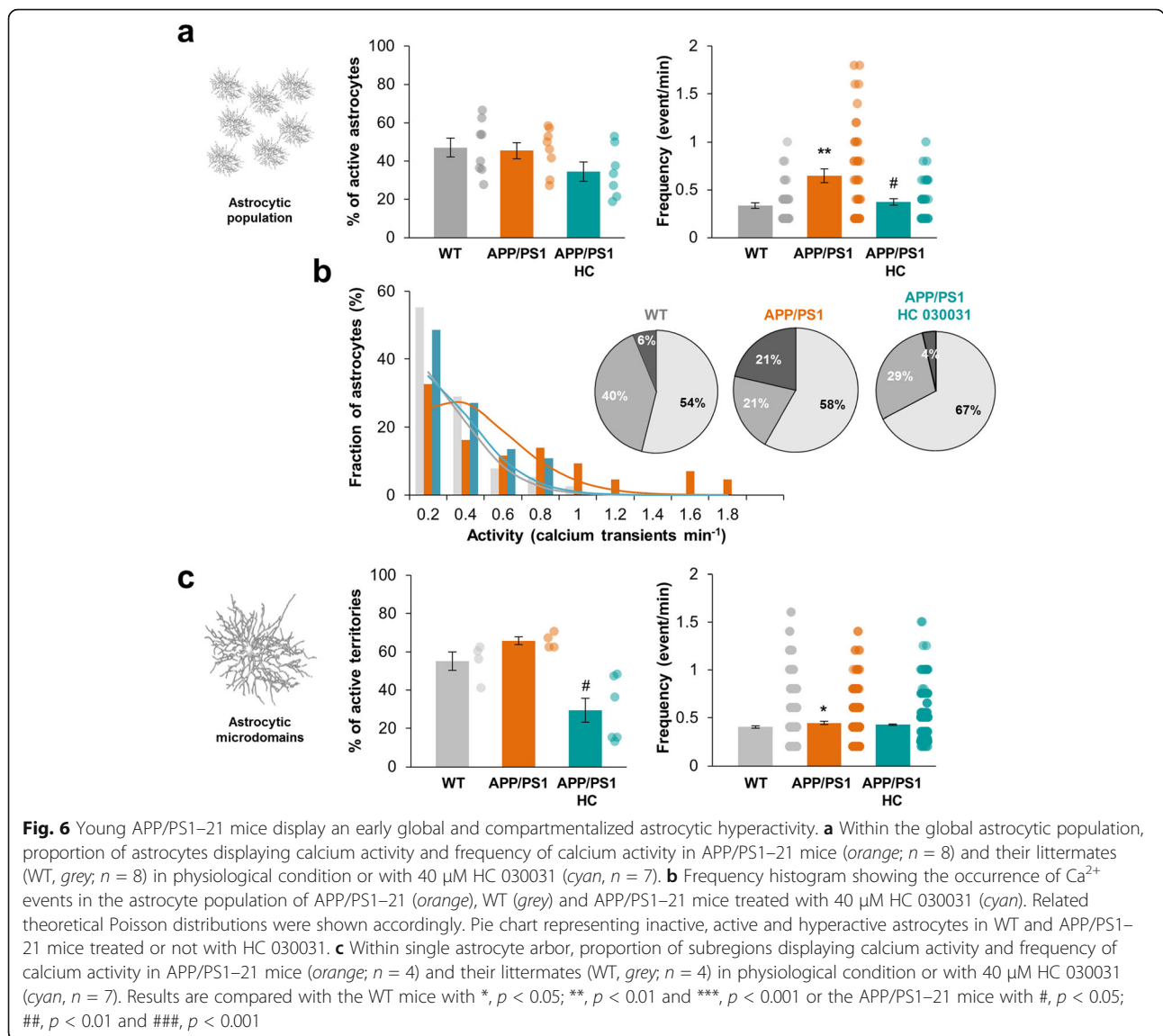


**Fig. 5** Young APP/PS1–21 mice are devoid of amyloid deposit and reactive astrocyte whereas gradually overexpress TRPA1. **a** Thioflavin S staining for  $\beta$ -amyloid deposits (green) and NeuN immunostaining (magenta) in the hippocampus of 1-month-old (left) and 6-month-old (right) APP/PS1–21 mice showing the progression of the number of amyloid deposits. **b** GFAP (cyan) and NeuN (magenta) immunostainings in the stratum radiatum of a P30 WT (left) and APP/PS1–21 (right) mice. **c** Western-blot analysis of protein levels of TRPA1 channels in hippocampus extracts from P19 and P30 WT and APP/PS1–21 mice (3 different extracts of P30 WT and APP/PS1–21 mice are shown). Histogram showing quantification of TRPA1 channels expression normalized to protein loading levels ( $n = 6$  hippocampus in each group at P19 and 8 hippocampus in each group at P30). **d** Western-blot analysis of protein levels of GFAP in hippocampus extracts from P19 and P30 WT and APP/PS1–21 mice (extracts of same P30 lysates depicted in c are shown). Histogram showing quantification of GFAP expression normalized to protein loading levels ( $n = 7$  hippocampus in each group at P19 and P30). Results are compared with the WT mice with \*,  $p < 0.05$ ; \*\*,  $p < 0.01$  and \*\*\*,  $p < 0.001$

APP/PS1–21 mice ( $n = 6$  slices from 4 animals;  $p = 0.88$  and  $0.82$  respectively; Additional file 5c) testifying that microglia activation was not involved in the astrocytic hyperactivity setting up at the beginning of  $A\beta$  secretion in this AD mouse model. In patch-clamp loaded astrocyte, the proportion of active microdomains increased in APP/PS1–21 mice ( $65.7 \pm 2.0\%$  vs  $55.0 \pm 4.8\%$  in WT;  $n = 4$  astrocytes from 4 animals for each;  $p = 0.052$ ; Fig. 6c)

together with the frequency of events within these microdomains ( $0.45 \pm 0.02$  event/min vs  $0.40 \pm 0.01$  event/min in WT;  $n = 255$  and  $426$  ROIs respectively;  $p = 0.04$ ; Fig. 6c). The proportion of expanded/focal events was slightly affected in APP/PS1–21 mice in favor of expanded event and the size of expanded events was similar ( $6.8 \pm 0.3 \mu\text{m}^2$  in WT vs  $6.7 \pm 0.3 \mu\text{m}^2$  in APP/PS1–21;  $p = 0.42$ ; Additional



file 4b, d). Thus, in young APP/PS1–21 mice,  $\text{Ca}^{2+}$  activity in the global astrocytic population and the compartmentalized activity within the astrocytic arbor started to be affected from the beginning of  $\text{A}\beta$  overproduction.

In these conditions, blocking TRPA1 channels with HC 030031 (40  $\mu\text{M}$ ) in APP/PS1–21 mice strongly decreased the frequency of  $\text{Ca}^{2+}$  events ( $0.37 \pm 0.03$  event/min with HC 030031 vs  $0.64 \pm 0.07$ ;  $n = 113$  astrocytes from 7 slices;  $p = 0.013$ ; Fig. 6a) resulting in a clear redistribution of  $\text{Ca}^{2+}$  events frequency ( $\lambda = 1.35$ ) and a decrease of the proportion of hyperactive cells that look alike the WT situation (4% in APP/PS1–21 + HC 030031 vs 21% in APP/PS1–21;  $p = 0.0025$ ; Fig. 6b). In patch-clamp loaded astrocyte, HC 030031 induced a significant decrease of the proportion of active microdomains in APP/PS1–21 mice ( $29.3 \pm 6.2\%$ ;  $n = 7$  from 4

animals;  $p = 0.01$ ; Fig. 6c) together with a restrained effect on the frequency ( $0.43 \pm 0.06$  event/min;  $n = 1213$  and 1577 ROIs respectively;  $p = 0.058$ ). The proportion of expanded/focal events was also reduced with HC 030031 treatment (Additional file 4b). Overall, these observations in young APP/PS1–21 mice matched the above related effect of  $\text{A}\beta$  application in healthy slices consistently with a TRPA1 channel involvement. Merely, they were more subtle and initially restrained to the astrocytic arbor.

#### **$\text{A}\beta$ -induced CA1 neurons hyperactivity is related to TRPA1 channels activation**

Astrocytes are known to actively regulate synaptic activity and plasticity [4]. Given the time range of the  $\text{A}\beta$ -mediated impact on astrocyte excitability, we wonder about its consequences on basal synaptic activity. Thus,

to explore the outcome of A $\beta$  induced TRPA1-dependent astrocyte hyperexcitability on neighboring synapses, we recorded CA1 pyramidal neurons spontaneous excitatory post-synaptic currents (sEPSCs) performing whole-cell patch-clamp recordings on CA1 neurons cell bodies (Fig. 7a). The initial mean frequency of sEPSCs recorded from CA1 pyramidal neurons was  $0.13 \pm 0.03$  Hz ( $n = 22$  neurons from 17 animals) and was stable during a 30-min recording (Fig. 7b). The mean peak amplitude of sEPSCs recorded from CA1 pyramidal neurons was  $31.1 \pm 2.0$  pA. Interestingly, application of 40  $\mu$ M HC 030031 alone had no effect on

sEPSCs frequency ( $74 \pm 22\%$  from 5 to 10 min;  $n = 5$  cells from 3 animals;  $p = 0.6$ ; Fig. 7b, c) suggesting that TRPA1 channels were not involved in physiological sEPSCs modulation. Application of 100 nM A $\beta$  in the extracellular medium induced a rapid, strong and persistent increase of sEPSCs frequency (Fig. 7b;  $n = 7$  cells from 6 animals) with no effect on the sEPSCs amplitude ( $32.4 \pm 2.5$  pA;  $p = 0.3$ ). We confirmed that application of monomeric forms of A $\beta_{1-42}$  (A $\beta$ m) had no effect on sEPSCs frequency during the 30-min recording ( $n = 5$ ;  $p = 0.78$ ; Additional file 1d) settling that only oligomeric forms of A $\beta_{1-42}$  were active. Interestingly, the strong

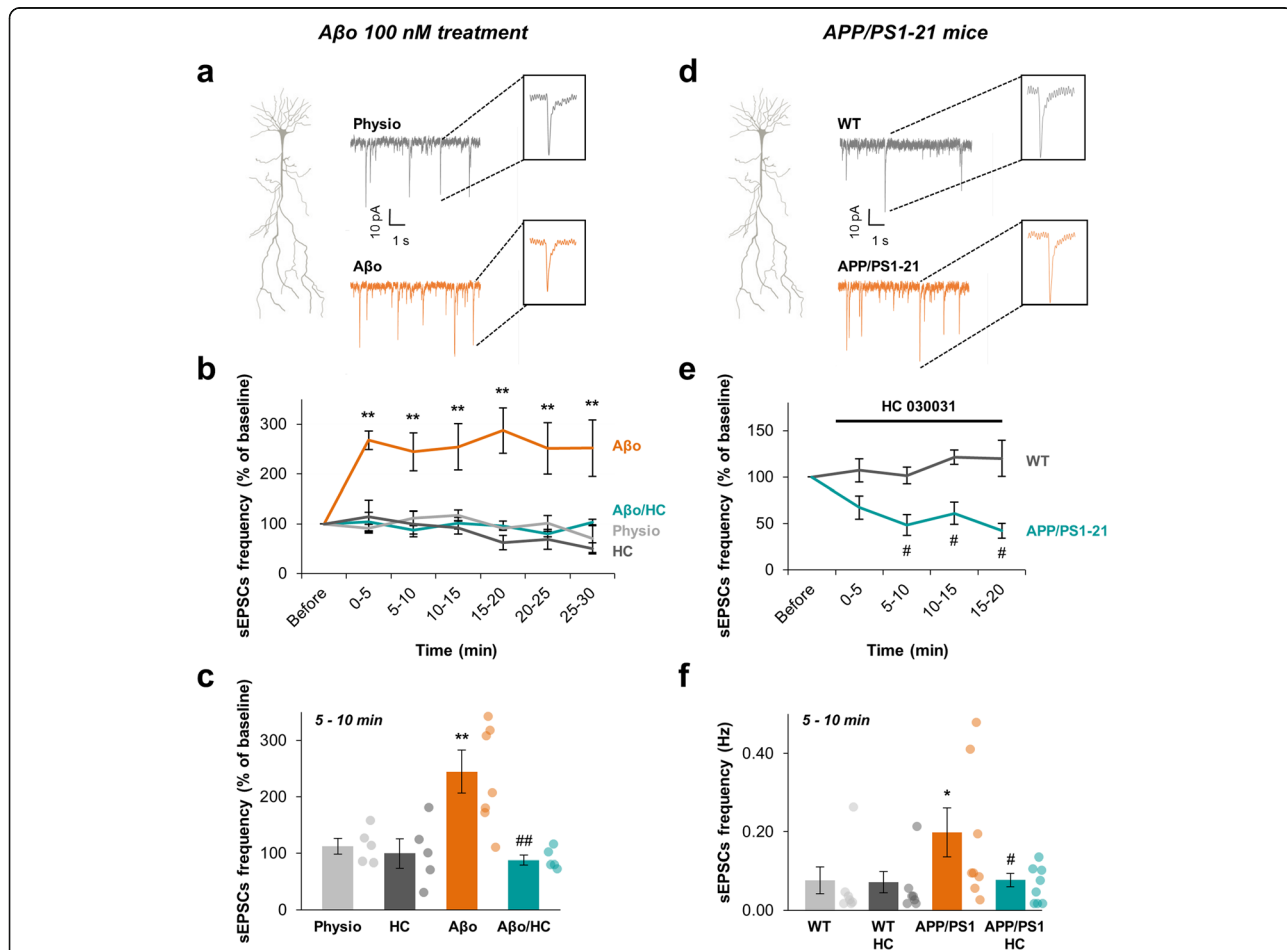


**Fig. 7** A $\beta$  increases the frequency of spontaneous excitatory post-synaptic currents (sEPSCs) from CA1 pyramidal neurons in a TRPA1 channels dependent manner. **a** Representative traces of voltage-clamp recordings from CA1 pyramidal cells held at  $-65$  mV in physiological condition (grey) and under A $\beta$  100 nM application (orange). Examples of single EPSC with higher time resolution are shown in the corresponding insets. **b** Time course of the frequency of sEPSCs in physiological condition (light grey;  $n = 5$ ), under application of 100 nM A $\beta$  (orange;  $n = 7$ ), 40  $\mu$ M HC 030031 (dark grey;  $n = 5$ ) or co-application of 100 nM A $\beta$  + 40  $\mu$ M HC 030031 (cyan;  $n = 4$ ). **c** Histogram showing the sEPSCs frequency at a time matching the astrocyte calcium activity measurements (i.e. 5 to 10 min after drugs application). Results are compared with the physiological condition with \*,  $p < 0.05$ ; \*\*,  $p < 0.01$  and \*\*\*,  $p < 0.001$  or the A $\beta$  condition with #,  $p < 0.05$ ; ##,  $p < 0.01$  and ###,  $p < 0.001$ . **d** Representative traces of voltage-clamp recordings from CA1 pyramidal cells held at  $-65$  mV in APP/PS1-21 mice (orange) and their WT littermates (grey). Examples of single EPSC with higher time resolution are shown in the corresponding insets. **e** Time course of the normalized frequency of sEPSCs in WT (dark grey;  $n = 7$ ) and APP/PS1-21 mice (cyan;  $n = 8$ ) under application of 40  $\mu$ M HC 030031. **f** Histogram showing the sEPSCs frequency in basal condition in WT (light grey;  $n = 7$ ), APP/PS1-21 mice (orange;  $n = 8$ ) and 5 to 10 min after HC 030031 application (dark grey and cyan respectively). Results are compared to the WT basal activity with \*,  $p < 0.05$ ; \*\*,  $p < 0.01$  and \*\*\*,  $p < 0.001$  or the APP/PS1-21 basal activity with #,  $p < 0.05$ ; ##,  $p < 0.01$  and ###,  $p < 0.001$

and persistent increase of sEPSCs frequency induced by A $\beta$  was time-concomitant with the setting up of astrocyte hyperexcitability (i.e. 5 to 10 min,  $245 \pm 38\%$ ;  $p = 0.01$ ; Fig. 7c) and was fully abolished by a co-application of HC 030031 (40  $\mu$ M) with A $\beta$  ( $88 \pm 8\%$  from 5 to 10 min;  $n = 5$  cells from 5 animals;  $p = 0.005$ ; Fig. 7b, c). This suggests that TRPA1 channels-dependent astrocyte hyperactivity induced by A $\beta$  directly influenced CA1 neurons activity and its blockade was enough to counteract the neuronal hyperactivity, at least in the short and medium term.

We then recorded spontaneous EPSCs in APP/PS1–21 mice at the onset of A $\beta$  overproduction (P20–P28) and compared to their littermates (WT). We observed an increase of CA1 neurons sEPSCs frequency setting up at P20 in APP/PS1–21 mice ( $0.20 \pm 0.06$  Hz in APP/PS1–21 vs  $0.08 \pm 0.03$  Hz in WT;  $n = 8$  neurons from 6 animals in APP/PS1–21 and 7 neurons from 5 animals in WT;  $p = 0.0271$ ; Fig. 7d, f) with no difference in their amplitude ( $33.7 \pm 1.9$  pA in APP/PS1–21 vs  $33.0 \pm 2.3$  pA in WT;  $p = 0.955$ ). These data confirmed that neuronal hyperexcitability is one of the earliest dysfunction in the pathophysiological cascade initiated by abnormal A $\beta$  accumulation [32]. Application of HC 030031 (40  $\mu$ M) strongly reduced sEPSCs frequency in APP/PS1–21 mice as soon as 5 min after its bath perfusion ( $0.08 \pm 0.02$  Hz;  $n = 8$  neurons from 6 animals;  $p = 0.0234$ ) while it had no effect on WT mice ( $0.07 \pm 0.03$  Hz;  $n = 7$  neurons from 5 animals;  $p = 0.854$ ; Fig. 7e, f). These data corroborate the highlighted precocious involvement of TRPA1 channel in AD pathogenesis.

## Discussion

In this study, we investigated the contribution of astrocytes in early A $\beta$  toxicity by studying calcium signaling in different parts of the whole astrocyte territory. We found that astroglia is a frontline target of A $\beta$  exhibiting a global and local Ca $^{2+}$  hyperactivity that involves TRPA1 channels. This TRPA1 channel-dependent astrocytic Ca $^{2+}$  hyperactivity exerts regulatory influences on synaptic function and is linked to the glutamatergic synapse hyperactivity recorded in CA1 neurons. Concurrently to these acute A $\beta$ -induced effects, astrocytes in young APP/PS1–21 mice hippocampus elicit a similar pattern of calcium hyperactivity in close relationship with the setting up of a precocious neuronal hyperactivity that are both reversed when TRPA1 channel is blocked. Moreover, the TRPA1 channel is gradually over-expressed at the onset of A $\beta$  production in this AD mouse model.

Intracellular Ca $^{2+}$  transients are considered as the primary signal by which astrocytes interact with each other and with neighboring neurons. Ca $^{2+}$  has been extensively

studied within the astrocytic cell body and thick branches. More recently, local Ca $^{2+}$  dynamics in distal fine processes has been investigated emphasizing a highly compartmentalized signaling, interconnected with physiological transmission at neighboring synapses [8, 9]. Compartmentalization of astrocytic Ca $^{2+}$  dynamics needs to be attentively considered in order to understand how astrocytes may contribute to brain information processing [8]. We thus chose to study both levels of information (i.e. global population signaling and local microdomain signaling) combining bulk loading and single cell astrocyte loading. Genetically encoded Ca $^{2+}$  indicators (GECIs) have been recently used to study Ca $^{2+}$  signals in distal thin processes [9]. Alternatively, patch pipette loading give access to the whole territory of a single astrocyte and, currently, Fluo-4 is far more sensitive than GECIs therefore enabling to track smaller signals [8]. Accordingly, we observed a similar and even better diffusion of Fluo-4 in a single astrocyte compared to SR101. We first characterized the physiological calcium activity of mouse CA1 *stratum radiatum* astrocytes and showed that this activity is fully autonomous, i.e. independent of neuronal activity, both at the astrocytic population level and at the microdomain level. This is in agreement with data obtained in mouse CA1 hippocampus [30, 33] but not with astrocyte behavior in the dentate gyrus where expanded Ca $^{2+}$  events were partly dependent on neuronal activity [8]. Interestingly, external Ca $^{2+}$  entry is the main source of Ca $^{2+}$  within thin processes whereas it only partly contributes to somatic signaling. This discrepancy between Ca $^{2+}$  sources in astrocyte soma and distal processes has already been described in brain slices [34]. This might be supported by the subcellular location of calcium stores that are concentrated in the cell body and thick processes but are almost absent from thin processes [23].

A central element of the pathogenesis of AD is the progressive accumulation of A $\beta$  species, ultimately resulting in the formation of plaques. Yet, small soluble A $\beta$  oligomers are sufficient to induce several features of the AD phenotype [1]. The paths by which A $\beta$  leads to neurodegeneration are probably multifactorial but all converge all towards synaptic dysfunction. The major challenge of AD research is to understand the complex cellular reaction underlying the long prodromal phase of AD [14]. Astrocytes are an integral part of synaptic transmission and are therefore critical for the establishment and maintenance of neuronal health [5]. They contribute to neuronal dysfunction by being proinflammatory [35] but also play a protective role, e.g. through the release of gliotransmitters [36] and A $\beta$  clearance [37, 38]. It is therefore of major importance to distinguish the beneficial

from the deleterious impact of A $\beta$  on astrocyte function. A $\beta$  has already been involved as a direct effector on astrocytes in primary cultures [39], in hippocampal slices [40] and in vivo [12] but here we showed a peculiar rapid action on compartmentalized calcium activity, activating a membrane Ca<sup>2+</sup> permeable channel. Indeed, A $\beta$  application triggers global Ca<sup>2+</sup> hyperactivity in CA1 hippocampus astroglial population together with an intensification of the compartmentalized Ca<sup>2+</sup> activity in the astrocytic processes and a spatial extension of the size of the expanded Ca<sup>2+</sup> events within microdomains. These effects are specific to oligomeric forms of A $\beta$  since application of the monomeric form in the same conditions had no impact on astrocytic calcium activity. We reported that the effect of A $\beta$  on astrocyte excitability is fully independent of neuronal activity since TTX application does not prevent the A $\beta$  effect neither on the global hyperactivity nor on the compartmentalized hyperactivity in processes. Concurrently, microglia activation does not participate in this astrocytic hyperactivity, at least in the time scale studied, whereas longer applications of A $\beta$  activate microglia together with astroglia [24]. Thus, astrocytes seem to express a distinctive precocious detector involved at the onset of A $\beta$  appearance. Removal of external Ca<sup>2+</sup> largely inhibits A $\beta$ -induced astrocyte hyperactivity at the population level while it has no effect in physiological conditions. Removal of external Ca<sup>2+</sup> also inhibits the majority of the compartmentalized A $\beta$ -induced hyperactivity. Thus, transmembrane Ca<sup>2+</sup> entry carries most of the A $\beta$ -induced hyperactivity. Remarkably, we showed that both global and compartmentalized hyperactivities are driven by TRPA1-dependent Ca<sup>2+</sup> entry since HC 030031, a specific TRPA1 channel inhibitor [29], strongly abolishes A $\beta$ -induced astrocyte hyperexcitability and totally restores the spatiotemporal properties of Ca<sup>2+</sup> events back to a physiological level.

The TRPA1 channel is a Ca<sup>2+</sup> permeable non-selective cation channel initially known to be expressed in primary afferent nociceptive neurons [29]. In mouse CA1 hippocampus, TRPA1 channels are found to be preferentially expressed in astrocytes [10]. However, their involvement in physiological astrocytic Ca<sup>2+</sup> signaling is highly debated. It has been shown that TRPA1 channels contribute to maintain basal Ca<sup>2+</sup> levels and regulate ~20% of spontaneous Ca<sup>2+</sup> signals within astrocyte branches [11] but in the end, poorly take part in basal astrocytic Ca<sup>2+</sup> signaling [30, 33]. Our data assume that TRPA1 channels are only slightly involved in the astrocytic Ca<sup>2+</sup> signaling in physiological conditions. However, we highlighted they are quickly and largely involved in case of A $\beta$  presence. The absence of an obvious involvement of these channels in astrocyte physiological Ca<sup>2+</sup> signaling is startling since we evidenced a TRPA1 channel expression in thick and in adjacent thin

astrocytic processes. Thus, TRPA1 channels might only behave as an “aggression sensor”. Indeed, TRPA1 channel gating is particularly regulated by numerous electrophilic activators - such as reactive oxygen species, reactive nitrogen species or oxidized lipids - and also functions as a mechanosensor [27]. Hence, TRPA1 channels might be directly targeted by A $\beta$  or might be secondarily activated through an A $\beta$ -induced oxidative stress and/or through its mechanosensor properties if A $\beta$  binds to the astrocytic cholesterol-rich plasma membrane [14].

Strikingly, in young APP/PS1-21 mice (~3–4 weeks), we observed a similar pattern of astrocytic hyperactivity starting at the beginning of A $\beta$  overproduction in the hippocampus, long before its aggregation into plaques. These early repercussions in young APP/PS1-21 mice were restricted to the frequency of astrocytic Ca<sup>2+</sup> events in either the astrocytic population and microdomains of astrocytic processes with fewer impacts on the proportion of active cells or microdomains. This suggests a gradual impact of surrounding A $\beta$  on astrocyte signaling, increasing the frequency of compartmentalized Ca<sup>2+</sup> events and, to a lesser extent, the proportion of active territories within the astrocytic processes. These impacts on astrocytic processes go along with a noteworthy redistribution of the frequency of Ca<sup>2+</sup> events within the astrocytic population. Interestingly, blockade of TRPA1 channels with HC 030031 abolished the astrocyte Ca<sup>2+</sup> hyperactivity. Overall, TRPA1 channel signaling seems to be at the frontline in mediating these A $\beta$  progressive effects in early stages of AD. Data obtained in an advanced AD transgenic model showed an astrocyte network hyperactivity in cortical areas close to A $\beta$  plaques and an involvement of metabotropic purinergic signaling in this astrocyte hyperactivity [13]. This suggests a differential evolution of astrocyte engagement in AD pathogenesis depending on the stage, the structure and the physiopathological state of the astrocyte. Likewise, it has been reported that the TRPA1 channels' protein level was increased in hippocampal astrocytes of 8 month-old APP/PS1 mice at where it mediated inflammation through astrocyte activation [41]. Here, we showed that TRPA1 channel expression in hippocampus is increased much earlier, as soon as 1 month of age, in a more aggressive AD mouse model (APP/PS1-21). These data point towards a TRPA1 channel contribution in early stages of pathophysiology, that is as soon as the A $\beta$  level increases and long before the setting up of astrogliosis or inflammatory mechanisms.

Numerous laboratory studies in the past decade have shown that A $\beta$  impairs synaptic function and synaptic structure [42]. However, how soluble A $\beta$  initiates these effects remains to be determined. Each astrocyte deploys many fine processes to contact up to 140,000 synapses in the CA1 region [43]. As we highlighted an intense



and early effect of A $\beta$  on astrocyte Ca<sup>2+</sup> activity within processes, we assessed the link with spontaneous neuronal activity. Indeed A $\beta$  is also known to enhance spontaneous neuronal excitability in CA1 [32, 44, 45]. Consistently, we showed here that A $\beta$  induces a rapid and strong increase of spontaneous EPSCs frequency in CA1 neurons. Strikingly, blocking TRPA1 channels totally prevents this A $\beta$  neuronal impact. Yet, when we blocked neuronal activity with TTX, we did not affect the A $\beta$ -induced astrocyte hyperactivity which would be partly the case if a neuronal TRPA1 was involved. This precocious A $\beta$  impact thus seems to trigger a one-way communication from astrocyte to neuron related to TRPA1 activation. This TRPA1-dependent neuronal hyperactivity was similarly observed in APP/PS1–21 mice at the onset of A $\beta$  overproduction testifying its pathophysiological relevance in the AD initiation process. It has been shown that A $\beta$  can increase astrocytic release of glutamate to the extrasynaptic space resulting in the activation of extrasynaptic NMDARs and the disruption of neuronal signaling [40, 46, 47]. Besides, astrocytes can regulate synaptic and extrasynaptic neurotransmitter concentrations, such as glutamate, in a Ca<sup>2+</sup>-dependent manner e.g. via vesicular release, bidirectional transport or hemichannel opening [48]. We will further decipher pathways implemented by the A $\beta$ -induced TRPA1-mediated Ca<sup>2+</sup> entry that consequently affect neuronal transmission.

It has been demonstrated that soluble A $\beta$  can affect astrocyte signaling properties in various ways in mouse hippocampal CA1 astrocytes [40, 49, 50]. To some extent, the involvement of TRPA1 channels superimposed to these effects, directly affecting local synaptic function in a distinctive precocious manner. This actor might thus contribute to the complex cellular phase of AD, upstream of symptomatic neurodegeneration [14].

## Conclusions

In this work, we have shown that intricate global and compartmentalized astroglial Ca<sup>2+</sup> signaling disturbances induced by A $\beta$  are mediated by a TRPA1 channel-dependent Ca<sup>2+</sup> signaling. This new highlighted mechanism is at work with both external supply of A $\beta$  and at the onset of A $\beta$  production in an AD transgenic mouse model. This astrocytic pathway is promptly implemented and involved in the well-known and characteristic A $\beta$ -induced synaptic dysfunction. Blockade of TRPA1 channel, that appears to be preferentially expressed in astrocytes within the hippocampus [11], is sufficient to counteract the impact of A $\beta$  on spontaneous neuronal activity. This suggests that astrocytes can be considered as a particularly precocious target in A $\beta$  toxicity consequently affecting nearby synapses. Up until now, altered astrocyte activation was usually associated with late AD,

i.e. when amyloid plaques are already developed, and the role of astrocytes in the initial toxic effect of A $\beta$  was not yet evidenced. One of the major findings of our study is to suggest that astrocytes are implicated far before astrogliosis and inflammatory processes. Thus, focusing on this astrocyte involvement, for instance by modulating TRPA1 channel activity, may represent a novel target to hamper early dysfunction in AD.

## Additional files

**Additional file 1:** Characterization and effects of A $\beta$  oligomers and purified monomers. **(a)** SDS-PAGE analysis of A $\beta$  oligomers examined by western-blot with 4G8 antibody. A $\beta$  showed faintly monomers and abundant dimers and trimers. **(b)** SDS-PAGE analysis of A $\beta$  monomers after purification on C18 column. All fractions were electrophoresed on 15% tris-glycine gel. A $\beta$  monomer is mainly eluted at 30% acetonitrile. S, sample loaded; FT, flow through; peptides eluted at 30, 40, 50 and 60% acetonitrile. **(c)** Within the astrocytic population, proportion of astrocytes displaying calcium activity and frequency of astrocyte calcium activity in physiological condition (grey; n = 43), under 100 nM A $\beta$  application (orange; n = 12) and under 100 nM A $\beta$ m application (light orange; n = 7). **(d)** Time course and histogram at 5–10 min of the frequency of sEPSCs in physiological condition (grey; n = 5), under application of 100 nM A $\beta$  (orange; n = 7) or 100 nM A $\beta$ m (light orange; n = 5). In any case, A $\beta$ m was obtained from the 30% acetonitrile fraction purified in b. (TIFF 291 kb)

**Additional file 2:** Characterization of Fluo-4-loaded cells in the *stratum radiatum* of mouse coronal slice. **(a)** Confocal image of Fluo-4-loaded (cyan) and SR101-labeled (magenta) cells in the CA1 *stratum radiatum*. Merged image showing the proportion of loaded astrocytes (white), confirming that most of the loaded cells are astrocytes. One hour before slicing, animals were iv injected with SR101 as described previously [51]. Vessels are only labeled with SR101 (white arrow). **(b)** Z-stack projections of confocal images of a patched astrocyte loaded with Fluo-4 (cyan) and SR101 (magenta). Merged image showing the Fluo-4 diffusion in the whole astrocytic territory. **(c)** Example of a passive whole-cell current recorded in a *stratum radiatum* astrocyte. Cell was held at –70 mV and 10 mV hyper- and depolarizing voltage steps of 80 ms duration were applied (–110 to +80 mV). (TIFF 1907 kb)

**Additional file 3:** Expanded and focal Ca<sup>2+</sup> events in astrocytic processes. Time-lapse imaging of calcium activity in Fluo-4 loaded astrocytic processes in a 5-min recording. Focal and expanded events were pseudo-colored in blue and red respectively (left panel). Raw data were shown in the right panel. (MP4 10286 kb)

**Additional file 4:** Spatial properties of compartmentalized calcium events in the astrocytic processes. **(a)** Proportion of expanded/focal events in physiological condition, under 100 nM A $\beta$  application, 100 nM A $\beta$  + 500 nM TTX co-application and 100 nM A $\beta$  + 40  $\mu$ M HC 030031 co-application. **(b)** Proportion of expanded/focal events in APP/PS1–21 mice and their littermates (WT) in physiological condition or under 40  $\mu$ M HC 030031 treatment. **(c)** Mean size of expanded Ca<sup>2+</sup> events in physiological condition (grey), under 100 nM A $\beta$  application (orange), 100 nM A $\beta$  + 500 nM TTX co-application (dark blue), 40  $\mu$ M HC 030031 (dark grey), 100 nM A $\beta$  in Ca<sup>2+</sup>-free medium application (0 Ca; light blue) and 100 nM A $\beta$  + 40  $\mu$ M HC 030031 co-application (cyan). **(d)** Mean size of expanded Ca<sup>2+</sup> events in APP/PS1–21 mice (orange) and their littermates (WT, light grey) in physiological condition or with 40  $\mu$ M HC 030031 treatment (WT, dark grey and APP/PS1–21, cyan). Results are compared with the physiological condition with \*, p < 0.05; \*\*, p < 0.01 and \*\*\*, p < 0.001 or the A $\beta$  condition with #, p < 0.05; ##, p < 0.01 and ###, p < 0.001. (TIFF 752 kb)

**Additional file 5:** Blockade of microglia activation with minocycline does not prevent the effect of A $\beta$  on astrocyte Ca<sup>2+</sup> activity. **(a)** Within the astrocytic population, proportion of astrocytes displaying calcium activity and frequency of astrocyte calcium activity in physiological

condition (grey;  $n = 43$ ), under 50 nM minocycline (dark grey;  $n = 5$ ); 100 nM A $\beta$  application (orange;  $n = 12$ ) and under 50 nM minocycline +100 nM A $\beta$  application (dark orange;  $n = 6$ ). **(b)** Immunohistochemistry of mouse *stratum radiatum* microglia showing that Iba1-positive cells were not hypertrophic in one-month-old APP/PS1–21 mice when compared to WT littermates. Higher magnification of representative microglia is shown in the lower panels. **(c)** Proportion of astrocytes displaying calcium activity and frequency of astrocyte calcium activity in APP/PS1–21 mice (orange;  $n = 8$ ), under 50 nM minocycline application (dark orange;  $n = 6$ ) or in WT littermates (grey;  $n = 8$ ). Minocycline is pre-incubated 15 min before recording. Results are compared with the physiological condition, with or without minocycline, or with the WT littermates with \*,  $p < 0.05$ ; \*\*,  $p < 0.01$  and \*\*\*,  $p < 0.001$ . (TIFF 1680 kb)

**Additional file 6:** TRPA1 is expressed in *stratum radiatum* astrocyte cell body and processes. **(a)** Immunohistochemistry of mouse *stratum radiatum* astrocytes showing that TRPA1 channels (green) are expressed within astrocytic domains certified by GFAP staining (magenta). **(b)** Merge image showing that most TRPA1 staining co-localized and surrounded GFAP-positive processes. (TIFF 2786 kb)

**Additional file 7:** TRPA1 channels expression is located in thick GFAP-positive processes and in adjacent thin processes lacking GFAP staining. 3D-reconstruct of astrocytic processes objectivized by GFAP staining (magenta) showing that TRPA1 channels (green) expression went over in contiguous processes excluding GFAP staining. Scale bar: 50 nm. (MP4 25.2 mb)

#### Abbreviations

AD: Alzheimer's disease; APP: Amyloid Precursor Protein; A $\beta$ : Amyloid- $\beta$  peptide; A $\beta$ m: Amyloid- $\beta$  monomers; A $\beta$ o: Amyloid- $\beta$  oligomers; Ca<sup>2+</sup>: calcium; CA1: Cornu Ammonis 1; GFAP: Glial Fibrillary Acidic Protein; PS1: Presenilin 1; ROI: Regions Of Interest; sEPSC: spontaneous Excitatory PostSynaptic Current; TRPA1: Transient Receptor Potential A1 channel; TTX: tetrodotoxin

#### Acknowledgements

We gratefully acknowledge Fabien Mehr and Flore Rimet for their technical assistance in animal perfusion, Rebecca Powell for correcting the english, Yasmına Saoudi for her technical assistance in Airyscan image acquisition on PIC-GIN platform of Grenoble Institut des Neurosciences, Dr. Jean-Claude Platel and Dr. Elodie Fino for stimulating scientific discussions.

#### Funding

This work was supported by INSERM and University Grenoble Alpes.

#### Availability of data and materials

All data generated or analyzed during this article are included in this published article and its additional information files.

#### Authors' contributions

ABo performed the calcium imaging experiments. AP carried out the electrophysiological experiments and contributed to some calcium imaging experiments. SB performed the immunoblotting and immunohistochemistry experiments. MJ-S carried out purification of A $\beta$  monomeric forms. ABo, ABu and MA designed the experiments. ABo, AP, SB and MA analyzed the data. ABo and MA wrote the manuscript. All authors discussed the results and commented on the manuscript at all stages. All authors read and approved the final manuscript.

#### Author's information

Not applicable.

#### Ethics approval

All experiments were carried out in accordance with the European Community Council directives of November 24, 1986 (86/609/EEC) and with the French guidelines on the use of living animals in scientific investigations with the approval of the "Grenoble Institute of Neurosciences Ethical Committee".

#### Consent for publication

Not applicable.

#### Competing interests

The authors declare that they have no competing interests.

#### Publisher's Note

Springer Nature remains neutral with regard to jurisdictional claims in published maps and institutional affiliations.

Received: 17 February 2017 Accepted: 29 June 2017

Published online: 06 July 2017

#### References

- Haass C, Selkoe DJ. Soluble protein oligomers in neurodegeneration: lessons from the Alzheimer's amyloid beta-peptide. *Nat Rev Mol Cell Biol*. 2007;8:101–12.
- Verkhratsky A, Steinhauser C. Ion channels in glial cells. *Brain Res Brain Res Rev*. 2000;32:380–412.
- Panatier A, Theodosis DT, Mothet JP, Touquet B, Pollegioni L, Poulain DA, et al. Glia-derived D-serine controls NMDA receptor activity and synaptic memory. *Cell*. 2006;125:775–84.
- Haydon PG. GLIA: listening and talking to the synapse. *Nat Rev Neurosci*. 2001;2:185–93.
- Araque A, Parpura V, Sanzgiri RP, Haydon PG. Tripartite synapses: glia, the unacknowledged partner. *Trends Neurosci*. 1999;22:208–15.
- Verkhratsky A, Reyes RC, Parpura V. TRP channels coordinate ion signalling in astroglia. *Rev Physiol Biochem Pharmacol*. 2014;166:1–22.
- Hausteiner MD, Kracun S, Lu X-H, Shih T, Jackson-Weaver O, Tong X, et al. Conditions and constraints for astrocyte calcium signaling in the hippocampal mossy fiber pathway. *Neuron*. 2014;82:413–29.
- Di Castro MA, Chuquet J, Liaudet N, Bhaukaurally K, Santello M, Bouvier D, et al. Local Ca<sup>2+</sup> detection and modulation of synaptic release by astrocytes. *Nat Neurosci*. 2011;14:1276–84.
- Shigetomi E, Bushong EA, Hausteiner MD, Tong X, Jackson-Weaver O, Kracun S, et al. Imaging calcium microdomains within entire astrocyte territories and endfeet with GCaMPs expressed using adeno-associated viruses. *J Gen Physiol*. 2013;141:633–47.
- Shigetomi E, Tong X, Kwan KY, Corey DP, Khakh BS. TRPA1 channels regulate astrocyte resting calcium and inhibitory synapse efficacy through GAT-3. *Nat Neurosci*. 2012;15:70–80.
- Shigetomi E, Jackson-Weaver O, Huckstepp RT, O'Dell TJ, Khakh BS. TRPA1 channels are regulators of astrocyte basal calcium levels and long-term potentiation via constitutive D-serine release. *J Neurosci*. 2013;33:10143–53.
- Kuchibhotla K V, Lattarulo CR, Hyman BT, Bacskai BJ. Synchronous hyperactivity and intercellular calcium waves in astrocytes in Alzheimer mice. *Science* (80- ). 2009;323:1211–5.
- Delekate A, Fuchtemeier M, Schumacher T, Ulbrich C, Foddiss M, Petzold GC. Metabotropic P2Y1 receptor signalling mediates astrocytic hyperactivity in vivo in an Alzheimer's disease mouse model. *Nat Commun*. 2014;5:5422.
- De Strooper B, Karran E. The cellular phase of Alzheimer's disease. *Cell*. 2016;164:603–15.
- Radde R, Bolmont T, Kaeser SA, Coomaraswamy J, Lindau D, Stoltze L, et al. Abeta42-driven cerebral amyloidosis in transgenic mice reveals early and robust pathology. *EMBO Rep*. 2006;7:940–6.
- Barat E, Boisseau S, Bouyssières C, Appaix F, Savasta M, Albrieux M. Subthalamic nucleus electrical stimulation modulates calcium activity of nigral astrocytes. *PLoS One*. 2012;7:e41793.
- Reeves AM, Shigetomi E, Khakh BS. Bulk loading of calcium indicator dyes to study astrocyte physiology: key limitations and improvements using morphological maps. *J Neurosci*. 2011;31:9353–8.
- Nett WJ, Oloff SH, McCarthy KD. Hippocampal astrocytes in situ exhibit calcium oscillations that occur independent of neuronal activity. *J Neurophysiol*. 2002;87:528–37.
- Platel J-C, Dupuis A, Boisseau S, Villaz M, Albrieux M, Brocard J. Synchrony of spontaneous calcium activity in mouse neocortex before synaptogenesis. *Eur J Neurosci*. 2007;25:920–8.
- Stine WB, Dahlgren KN, Krafft GA, LaDu MJ. In vitro characterization of conditions for amyloid-beta peptide oligomerization and fibrillogenesis. *J Biol Chem*. 2003;278:11612–22.
- Apelt J, Schliebs R. Beta-amyloid-induced glial expression of both pro- and anti-inflammatory cytokines in cerebral cortex of aged transgenic Tg2576 mice with Alzheimer plaque pathology. *Brain Res*. 2001;894:21–30.

22. R Development Core Team. R: A language and environment for statistical computing. R Foundation for Statistical Computing, Vienna, Austria. (2008). ISBN 3-900051-07-0. <https://www.r-project.org/>.
23. Patrushev I, Gavrilov N, Turlapov V, Semyanov A. Subcellular location of astrocytic calcium stores favors extrasynaptic neuron-astrocyte communication. *Cell Calcium*. 2013;54:343-9.
24. Orellana JA, Shoji KF, Abudara V, Ezan P, Amigou E, Sáez PJ, et al. Amyloid  $\beta$ -induced death in neurons involves glial and neuronal hemichannels. *J Neurosci*. 2011;31:4962-77.
25. Abudara V, Roux L, Dall'érac G, Matias I, Dulong J, Mothet JP, et al. Activated microglia impairs neuroglial interaction by opening Cx43 hemichannels in hippocampal astrocytes. *Glia*. 2015;63:795-811.
26. Familian A, Boshuizen RS, Eikelenboom P, Veerhuis R. Inhibitory effect of minocycline on amyloid  $\beta$  fibril formation and human microglial activation. *Glia*. 2006;53:233-40.
27. Nilius B, Appendino G, Owsianik G. The transient receptor potential channel TRPA1: from gene to pathophysiology. *Pflügers Arch Eur J Physiol*. 2012;464:425-58.
28. Lee SM, Cho YS, Kim TH, Jin MU, Ahn DK, Noguchi K, et al. An ultrastructural evidence for the expression of transient receptor potential ankyrin 1 (TRPA1) in astrocytes in the rat trigeminal caudal nucleus. *J Chem Neuroanat*. 2012;45:45-9.
29. McNamara CR, Mandel-Brehm J, Bautista DM, Siemens J, Deranian KL, Zhao M, et al. TRPA1 mediates formalin-induced pain. *Proc Natl Acad Sci U S A*. 2007;104:13525-30.
30. Rungta RL, Bernier L-P, Dissing-Olesen L, Groten CJ, LeDue JM, Ko R, et al. Ca(2+) transients in astrocyte fine processes occur via Ca(2+) influx in the adult mouse hippocampus. *Glia*. 2016;
31. Porrero C, Rubio-Garrido P, Avendaño C, Clascá F. Mapping of fluorescent protein-expressing neurons and axon pathways in adult and developing Thy1-eYFP-H transgenic mice. *Brain Res*. 2010;1345:59-72.
32. Busche MA, Konnerth A. Neuronal hyperactivity - a key defect in Alzheimer's disease? *BioEssays*. 2015;37:624-32.
33. Nakayama R, Sasaki T, Tanaka KF, Ikegaya Y. Subcellular calcium dynamics during juvenile development in mouse hippocampal astrocytes. *Eur J Neurosci*. 2016;43:923-32.
34. Srinivasan R, Huang BS, Venugopal S, Johnston AD, Chai H, Zeng H, et al. Ca2+ signaling in astrocytes from *Ip3r2*<sup>-/-</sup> mice in brain slices and during startle responses in vivo. *Nat Neurosci*. 2015;18:708-17.
35. Orre M, Kamphuis W, Osborn LM, Jansen AHP, Kooijman L, Bossers K, et al. Isolation of glia from Alzheimer's mice reveals inflammation and dysfunction. *Neurobiol Aging*. 2014;35:2746-60.
36. Jung ES, An K, Hong HS, Kim J-H, Mook-Jung I. Astrocyte-originated ATP protects A $\beta$ (1-42)-induced impairment of synaptic plasticity. *J Neurosci*. 2012;32:3081-7.
37. Kraft AW, Hu X, Yoon H, Yan P, Xiao Q, Wang Y, et al. Attenuating astrocyte activation accelerates plaque pathogenesis in APP/PS1 mice. *FASEB J*. 2013;27:187-98.
38. Wyss-Coray T, Loike JD, Brionne TC, Lu E, Anankov R, Yan F, et al. Adult mouse astrocytes degrade amyloid-beta in vitro and in situ. *Nat Med*. 2003;9:453-7.
39. Grolla AA, Sim JA, Lim D, Rodriguez JJ, Genazzani AA, Verkhratsky A. Amyloid-beta and Alzheimer's disease type pathology differentially affects the calcium signalling toolkit in astrocytes from different brain regions. *Cell Death Dis*. 2013;4:e623.
40. Pirttimäki TM, Codadu NK, Awni A, Pratik P, Nagel DA, Hill EJ, et al.  $\alpha 7$  nicotinic receptor-mediated astrocytic gliotransmitter release: A $\beta$  effects in a preclinical Alzheimer's mouse model. *PLoS One*. 2013;8:e81828.
41. Lee K-I, Lee H-T, Lin H-C, Tsay H-J, Tsai F-C, Shyue S-K, et al. Role of transient receptor potential ankyrin 1 channels in Alzheimer's disease. *J Neuroinflammation*. 2016;13:92.
42. Mucke L, Selkoe DJ. Neurotoxicity of amyloid  $\beta$ -protein: synaptic and network dysfunction. *Cold Spring Harb Perspect Med*. 2012;2:a006338.
43. Bushong EA, Martone ME, Jones YZ, Ellisman MH. Protoplasmic astrocytes in CA1 stratum radiatum occupy separate anatomical domains. *J Neurosci*. 2002;22:183-92.
44. Varga E, Juhász G, Bozsó Z, Penke B, Fülöp L, Szegedi V. Abeta(1-42) enhances neuronal excitability in the CA1 via NR2B subunit-containing NMDA receptors. *Neural Plast*. 2014;2014:584314.
45. Lei M, Xu H, Li Z, Wang Z, O'Malley TT, Zhang D, et al. Soluble A $\beta$  oligomers impair hippocampal LTP by disrupting glutamatergic/GABAergic balance. *Neurobiol Dis*. 2016;85:111-21.
46. Talantova M, Sanz-Blasco S, Zhang X, Xia P, Akhtar MW, Okamoto S, et al. A $\beta$  induces astrocytic glutamate release, extrasynaptic NMDA receptor activation, and synaptic loss. *Proc Natl Acad Sci U S A*. 2013;110:E2518-27.
47. Kervern M, Angeli A, Nicole O, Leveille F, Parent B, Villette V, et al. Selective impairment of some forms of synaptic plasticity by oligomeric amyloid-beta peptide in the mouse hippocampus: implication of extrasynaptic NMDA receptors. *J Alzheimers Dis*. 2012;32:183-96.
48. Malarkey EB, Parpura V. Mechanisms of glutamate release from astrocytes. *Neurochem Int*. 2008;52:142-54.
49. Scimemi A, Meabon JS, Woltjer RL, Sullivan JM, Diamond JS, Cook DG. Amyloid- $\beta$ 1-42 slows clearance of synaptically released glutamate by mislocalizing astrocytic GLT-1. *J Neurosci*. 2013;33:5312-8.
50. Yi C, Mei X, Ezan P, Mato S, Matias I, Giaume C, et al. Astroglial connexin43 contributes to neuronal suffering in a mouse model of Alzheimer's disease. *Cell Death Differ*. 2016;7:1-11.
51. Girod S, Maurin M, van der Sanden B, Boisseau S, Appaix F, Guillemain I, et al. Specific in vivo staining of astrocytes in the whole brain after intravenous injection of sulforhodamine dyes. *PLoS One*. 2012;7:e35169.

Submit your next manuscript to BioMed Central and we will help you at every step:

- We accept pre-submission inquiries
- Our selector tool helps you to find the most relevant journal
- We provide round the clock customer support
- Convenient online submission
- Thorough peer review
- Inclusion in PubMed and all major indexing services
- Maximum visibility for your research

Submit your manuscript at [www.biomedcentral.com/submit](http://www.biomedcentral.com/submit)

